Supporting Information

Ancillary Ligands Tuned Ti(IV)-based Metallocalixarene Coordination Cages for Photocatalytic H_2 Evolution

Yi-Qi Tian,[a‡] Yun-Shu Cui,[b‡] Jia Hui-Zhu,[a] Cong-Qiao Xu,[b*] Xiao-Yi Yi,[a] Jun Li [b,c] and Chao Liu[a*]

[a] Hunan Provincial Key Laboratory of Chemical Power Sources, College of Chemistry and Chemical Engineering, Central South University, Changsha 410083, Hunan, P. R. China
[b] Department of Chemistry, Southern University of Science and Technology, Shenzhen 518055, P. R. China
[c]Department of Chemistry and Key Laboratory of Organic Optoelectronics & Molecular Engineering of Ministry of Education, Tsinghua University, 100084 Beijing, China

Corresponding Authors
*(Chao Liu) E-mail: chaoliu@csu.edu.cn
[†]Y.-Q.T. and Y.-S.C. contributed equally to this work

1. Experimental Section

Materials and Characterization. All reagents were purchased commercially and were not further purified when used. Powder X-ray diffraction (PXRD) analysis were performed on a Rigaku Mini Flex II diffractometer at a 2θ range of 3–50° (5° min^{-1}) with CuKα radiation (λ =1.54056 Å). The solid-state UV/Vis spectra data of the cluster samples were obtained on UV-4000 spectrophotometer. Electrospray ionization mass spectrometry (ESI-MS) were performed on a Bruker Daltonik GmbH (Bruker, Germany). Thermogravimetric (TGA) patterns were recorded on a Mettler Toledo TGA/SDTA 851e analyzer in a N_2 atmosphere. FT-IR spectra using KBr pellets were taken on a Bruker Vertex 70 Spectrometer.

Synthesis for compound {Ti(TBC[4])(O^iPr)}·$HNEt_3$·2^{i}PrOH {Ti-^{i}PrOH}: TBC[4] (21 mg, 0.032 mmol) were added in a 15mL reaction vessel with 3 mL isopropanol. Ti(O^iPr)$_4$ (100 μL, 0.33 mmol) and three drop triethylamine were added dropwise. The resulting mixtures were sonicated for 5 min, then were transferred to a preheated oven at 80 °C for 2 days. Yellow colored crystals were obtained after cooling to 25 °C in a yield of ~70%. Elem. Anal. Calcd for $C_{53}H_{74}O_5NTi$ (wt%): C, 74.62; H, 8.74; N, 1.64. Found: C, 73.91; H, 8.38; N, 1.31.

Synthesis for compound {H_2Ti_2(TBC[4])$_2$(MeO)$_2$}·4MeOH {Ti_2-MeOH}: TBC[4] (21 mg, 0.032 mmol) was added in a 15mL reaction vessel with 3 mL MeOH. Ti(O^iPr)$_4$ (100 μL, 0.33 mmol) was added dropwise. The resulting mixtures were sonicated for 5 min, then were transferred to a preheated oven at 80 °C for 2 days. Yellow colored crystals were obtained after cooling to 25 °C in a yield of ~70%. Anal. Calcd for $C_{90}H_{110}O_{10}Ti_2$ (wt%): C, 74.67; H, 7.66. Found: C, 73.82; H, 7.29.

Synthesis for compound {Ti_4O_2(O^iPr)$_4$(DMF)$_2$(TBC[4])$_2$} {Ti_4-DMF}: TBC[4] (21 mg, 0.032 mmol) were added in a 15mL reaction vessel with 3 mL DMF. Ti(O^iPr)$_4$ (100 μL, 0.33 mmol) was added dropwise. The resulting mixtures were then transferred to a preheated oven at 80 °C for 2 days. Yellow colored crystals were obtained after cooling to 25 °C in a yield of ~85%. Anal. Calcd for $C_{106}H_{142}N_2O_{16}Ti_4$ (wt%): C, 67.29; H, 7.56; N, 1.48. Found: C, 67.85; H, 7.23; N, 1.69.

Synthesis for compound {$H_2Ti_4O_2$(EtO)$_6$(TBC[4])$_2$} {Ti_4-EtOH}: TBC[4] (21 mg, 0.032 mmol) were added in a 15mL reaction vessel with 3 mL EtOH. Ti(O^iPr)$_4$ (100 μL, 0.33 mmol) was added dropwise. The resulting mixtures were then transferred to a preheated oven at 80 °C for 2 days. Yellow colored crystals were obtained after cooling to 25 °C in a yield of ~65%. Elem. Anal. Calcd for $C_{100}H_{138}O_{16}Ti_4$(wt%): C, 67.18; H, 7.78. Found: C, 67.56; H, 8.08.

Synthesis for compound {$Ti_4O_2(O^iPr)_4(TBC[4])_2$} {$Ti_4$-^{i}PrOH}: TBC[4] (21 mg, 0.032 mmol) were added in a 15mL reaction vessel with 3 mL ^{i}PrOH. $Ti(O^iPr)_4$ (100 μL, 0.33 mmol) was added dropwise. The resulting mixtures were then transferred to a preheated oven at 80 °C for 2 days. Yellow colored crystals were obtained after cooling to 25 °C in a yield of ~65%. Elem. Anal. Calcd for $C_{100}H_{132}O_{14}Ti_4$(wt%): C, 68.65; H, 7.60. Found: C, 68.26; H, 8.11.

Synthesis for compound {$Ti_{12}(O^iPr)_{12}(TBC[4])_6(Pdc)_6$}·14$CH_3CN$ {$Ti_{12}L_6$-1}: TBC[4] (30 mg, 0.046 mmol) and 3,5-pyridinedicarboxylic acid (H_2Pdc, 16.7 mg, 0.1 mmol) were added in a 15mL reaction vessel with 3 mL CH_3CN. $Ti(O^iPr)_4$ (100 μL, 0.33 mmol) was added dropwise. The resulting mixtures were then transferred to a preheated oven at 80 °C for 3 days. Red colored crystals were obtained after cooling to 25 °C in a yield of ~55%. Elem. Anal. Calcd for $C_{358}H_{438}N_{14}O_{60}Ti_{12}$(wt%): C, 66.43; H, 6.82; N, 3.02. Found: C, 67.35; H, 7.32; N, 3.52.

Synthesis for compound {$Ti_{12}(O^iPr)_{12}(TBC[4])_6(Pip)_6$}·34$CH_3CN$ {$Ti_{12}L_6$-2}: TBC[4] (42 mg, 0.065 mmol) and 5-(pyridin-4-yl)isophthalate (H_2Pip, 100 mg, 0.4 mmol) were sealed in a 25mL Teflon-lined reaction vesse with 5 mL CH_3CN. $Ti(O^iPr)_4$ (100 μL, 0.33 mmol) was added dropwise. The resulting mixtures were then transferred to a preheated oven at 100 °C for 3 days. Red colored crystals were obtained after cooling to 25 °C in a low yield of ~5%. **{$Ti_{12}L_6$-2}** has a low yield and coexists with other impurities. We can only manually pick a small number of crystals to do some basic characterization.

Photocurrent responses. Photoelectrochemical tests were carried out on a CHI 660E electrochemical workstation. The platinum plate was used as the counter electrode, and the saturated calomel electrode was used as the reference electrode. 5 mg crystal samples were ultrasonically dispersed in 1 ml ethanol, and then the dispersion was dropped on FTO glass to prepare the working electrode. The electrodes were immersed in the 0.2 M Na_2SO_4 aqueous solution. A 300 W Xe lamp with UV cut-off filter was used as a full-wavelength light source.

Contact Angle Measurements. Contact angles were measured on powder samples using a contact angle meter with a rotatable substrate holder. To perform contact angle measurements, 10 mg of powder samples of the clusters were deposited on a glass substrate bed. Then, powders were pressed to make a flat surface by the glass slide. A 10 μL water droplet was released slowly on the flat surface of the powder samples. The droplet image was taken by a high-performance charge-coupled device (CCD) sensor. The contact angle of all powder samples was analyzed by five-point simulation analysis.

H_2 Production Experiment. Photocatalytic hydrogen production tests were investigated in a closed gas circulation system (Beijing Perfect Light Co. Labsolar-III (AG)). Typically, 25 mg of cluster sample was dispersed in 30 mL of H_2O with 5 mL of triethanolamine (TEOA) as a sacrificial agent, and then 33 μL of 1.0 wt % H_2PtCl_6 was added. A 300 W Xe lamp was used as the UV−vis light source. Light passed through a UV cutoff filter ($\lambda > 420$ nm), and then the filtered light was focused onto the reactor. During irradiation, the headspace gas of the reactor was intermittently sampled every 30 min and H_2 from the headspace gas was monitored by a gas chromatograph (Shimadzu GC9860) equipped with a thermal conductivity detector, a 5A molecular sieve column, and Ar as carrier gas.

Theoretical and Computational Method Quantum chemistry calculations were performed using density functional theory (DFT). The generalized gradient approach with PBE exchange-correlation functional was adopted.[1] The uncontracted Slater TZP basis set was utilized for Ti atom and DZP basis sets for other elements in the calculations.[2] Frozen-core approximation was applied to [1s2] of O and [$1s^2$-$2p^6$] of Ti atoms. Scalar relativistic effect was accounted by zeroth order regular approximation (ZORA) approach.[3] All the calculations were done with ADF 2019.304 program.[4]

References:

1. J. P. Perdew, K. Burke, M. Ernzerhof. Generalized Gradient Approximation Made Simple. *Phys. Rev. Lett*., 1996, 77, 3865-3868.

2. E. V. Lenthe, E. J. Baerends, Optimized Slater-type basis sets for the elements 1-118, *J. Comput. Chem*. 2003, 24(9), 1142–1156.

3. E. V. Lenthe, R. V. Leeuwen, E. J. Baerends, J. G. Snijders, Relativistic regular two‐component Hamiltonians, *Int. J. Quantum Chem*. **1996**, 57(3), 281–293.

4. G. te Velde, F. M. Bickelhaupt, E. J. Baerends, C. Fonseca Guerra, S. J. A. van Gisbergen, J. G. Snijders, T. Ziegler. *J. Comput. Chem*. Chemistry with ADF, **2001**, 22(9), 931–967.

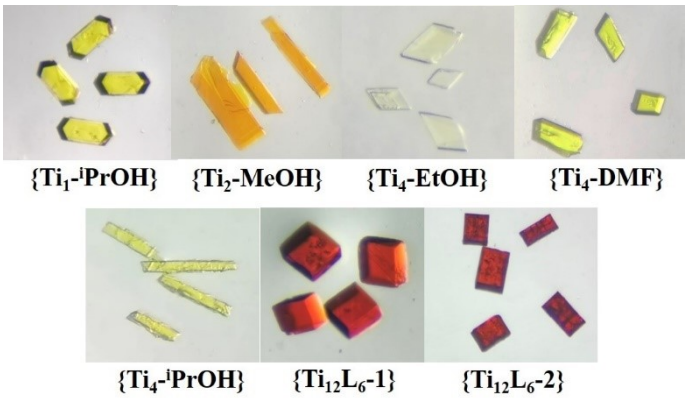

Figure S1. Pictures of fresh crystals separated from the solution.

2. Structure of Compounds

Compounds	**{Ti-^{i}PrOH}**	**{Ti_2-MeOH}**	**{Ti_4-DMF}**	**{Ti_4-EtOH}**
CCDC	**2101662**	**2101663**	**2101664**	**2101665**
Formula	$C_{60}H_{91}NO_7Ti$	$C_{94}H_{126}O_{14}Ti_2$	$C_{106}H_{142}N_2O_{16}Ti_4$	$C_{100}O_{16}H_{138}Ti_4$
T(K)	150	150	150	150
F_w	986.23	1575.74	1891.81	1783.66
Crystal system	monoclinic	monoclinic	triclinic	triclinic
Space group	$P2_1/c$	$P2_1/n$	P-1	P-1
a, Å	18.6310(2)	19.8135(4)	12.37700(10)	12.0088(4)
b, Å	12.8546(2)	22.9853(4)	12.6781(2)	12.1232(4)
c, Å	25.6170(3)	23.1531(4)	19.3873(2)	18.4541(5)
α/ °	90	90	90.5700(10)	80.451(3)
β/°	96.7860(10)	102.0212(17)	105.9730(10)	76.371(3)
γ/°	90	90	114.5140(10)	65.491(3)
V/Å^3	6092.14(14)	10313.1(3)	2634.17(6)	2368.67(15)
Z	4	4	1	1
ρ_{calcd}/gcm^{-3})	0.930	0.932	1.195	1.250
μ/mm^{-1})	1.471	1.668	2.978	3.274
F(000)	1844	3096.0	1012.0	950.0
Data/restraints/parameters	12707/153/674	21636/231/1193	10672/166/786	9191/136/725
Goof	1.065	1.029	1.042	1.075
R_1/wR_2(I> 2σ(I))	0.0764/0.2378	0.0648/0.1852	0.0537/0.1498	0.0541/0.1380
R_1/wR_2(all data)	0.0876/0.2561	0.0842/0.2004	0.0665/0.1568	0.0765/0.1518

Compounds	**{Ti_4-^{i}PrOH}**	**{$Ti_{12}L_6$-1}**	**{$Ti_{12}L_6$-2}**
CCDC	**2101666**	**2101668**	**2101669**
Formula	$C_{100}H_{132}O_{14}Ti_4$	$C_{370}H_{456}N_{20}O_{60}Ti_{12}$	$C_{443}H_{533}N_{40}O_{60}Ti_{12}$
T(K)	150.1	150.1	150.1
F_w	1749.65	6718.32	7952.59
Crystal system	triclinic	trigonal	monoclinic
Space group	P-1	R-3	$P2_1/c$
a, Å	15.0667(7)	33.1580(13)	24.2214(6)
b, Å	16.2142(8)	33.1580(13)	21.6454(4)
c, Å	21.1278(5)	31.9101(17)	42.7779(8)
α/ °	98.6700(3)	90	90
β/°	102.6620(4)	90	97.4170(2)
γ/°	101.7650(4)	120	90

V/Å^3	4825.8(4)	30383(3)	22240.0(8)
Z	2	3	2
ρ_{calcd}/gcm^{-3})	1.204	1.061	1.053
μ/mm^{-1})	3.188	0.286	2.233
F(000)	1864.0	10284.0	7462.0
Data/restraints/parameters	18948/67/1158	13149/105/758	39089/1048/2660
Goof	1.002	0.974	1.267
R_1/wR_2(I> 2σ(I))	0.0751/0.1832	0.0733/0.1857	0.1058/0.3227
R_1/wR_2(all data)	0.1463/0.2262	0.1211/0.2079	0.1249/0.3413

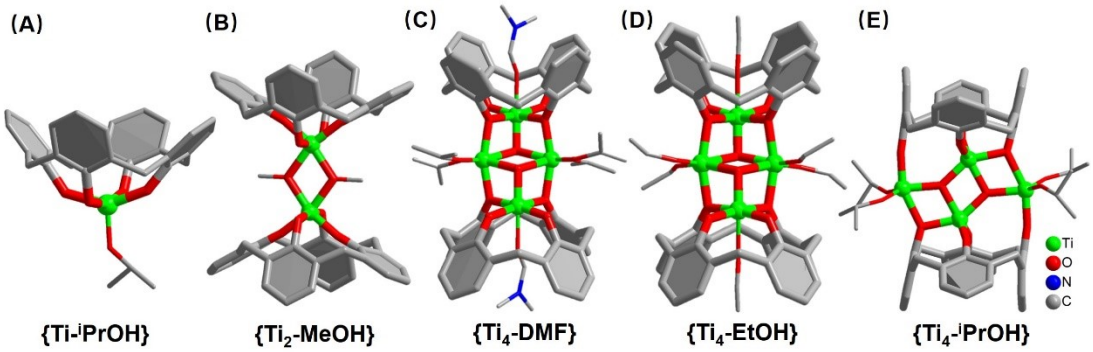

Figure S2. Structures of the simple TBC[4]-Ti clusters. The tert-butyl groups of TBC[4] ligands are deleted for brevity.

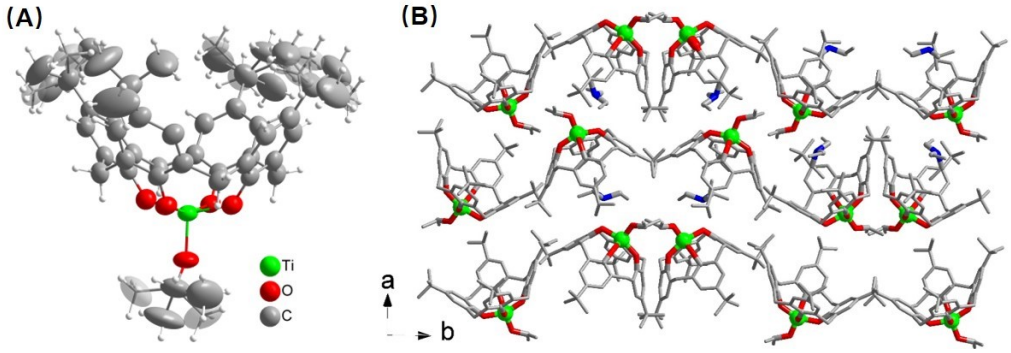

Figure S3. (A) ORTEP representation of the structure of **{Ti-^{i}PrOH}**; (B) Three-dimensional packing structure of **{Ti-^{i}PrOH}**.

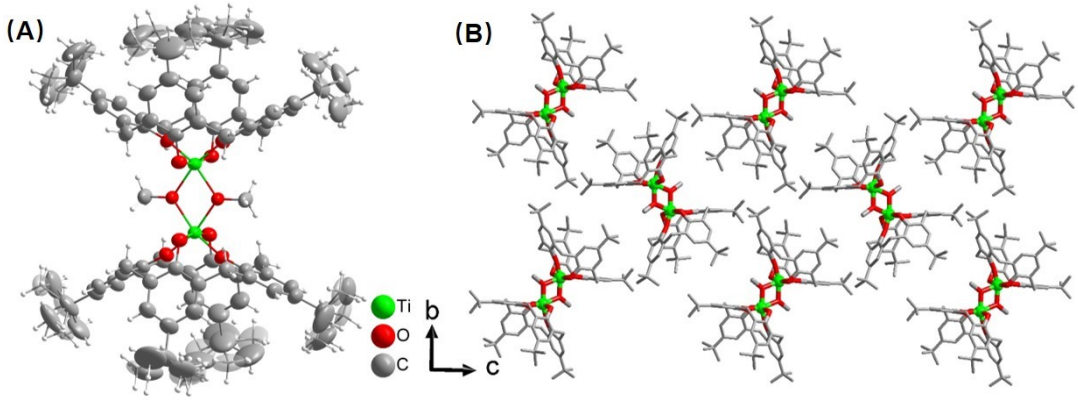

Figure S4. (A) ORTEP representation of the structure of **{Ti$_2$-MeOH}**; (B) Three-dimensional packing structure of **{Ti$_2$-MeOH}**.

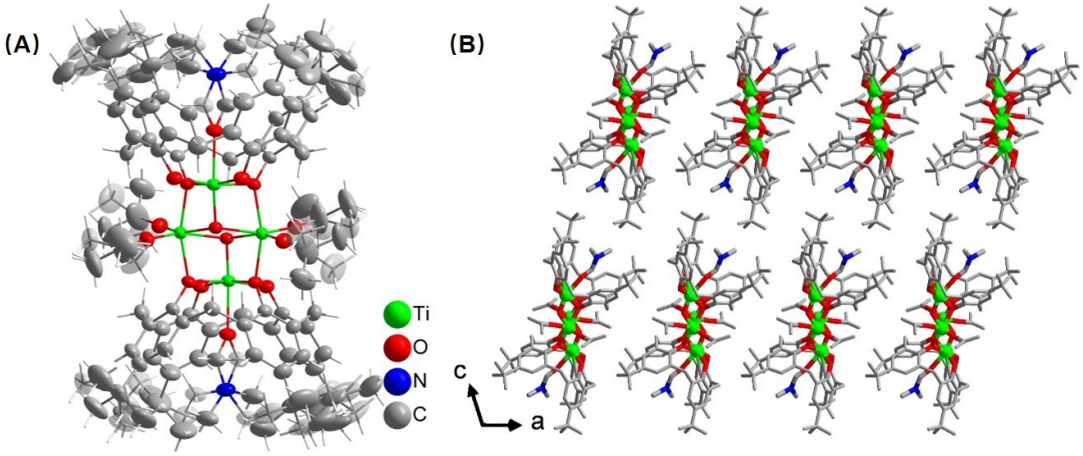

Figure S5. (A) ORTEP representation of the structure of **{Ti_4-DMF}**; (B) Three-dimensional packing structure of **{Ti_4-DMF}**.

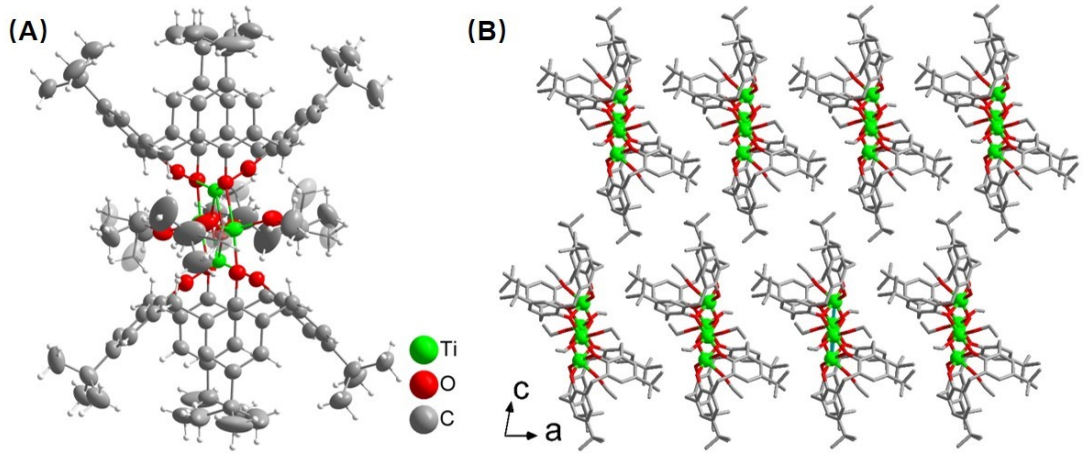

Figure S6. (A) ORTEP representation of the structure of **{Ti_4-EtOH}**; (B) Three-dimensional packing structure of **{Ti_4-EtOH}**.

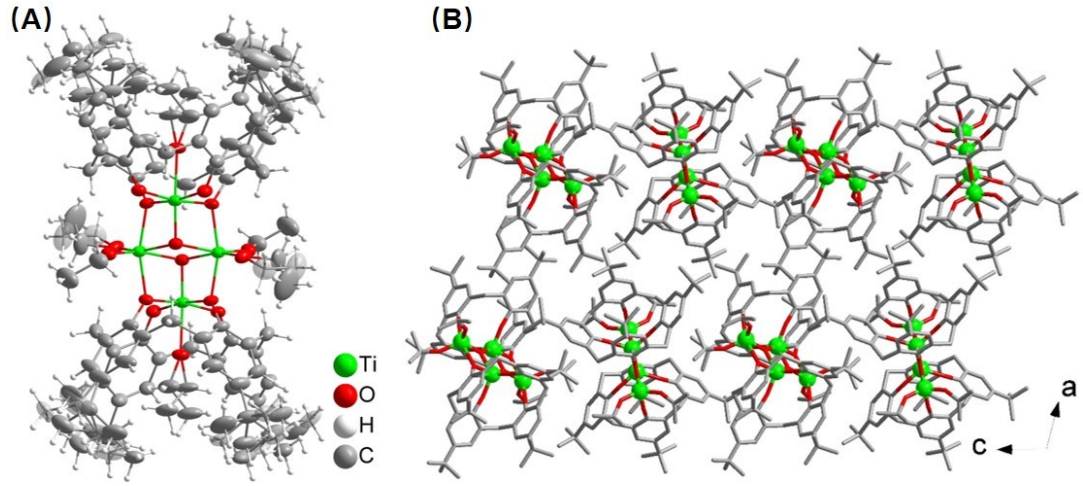

Figure S7. (A) ORTEP representation of the structure of **{Ti_4-^{i}PrOH}**; (B) Three-dimensional packing structure of **{Ti_4-^{i}PrOH}**.

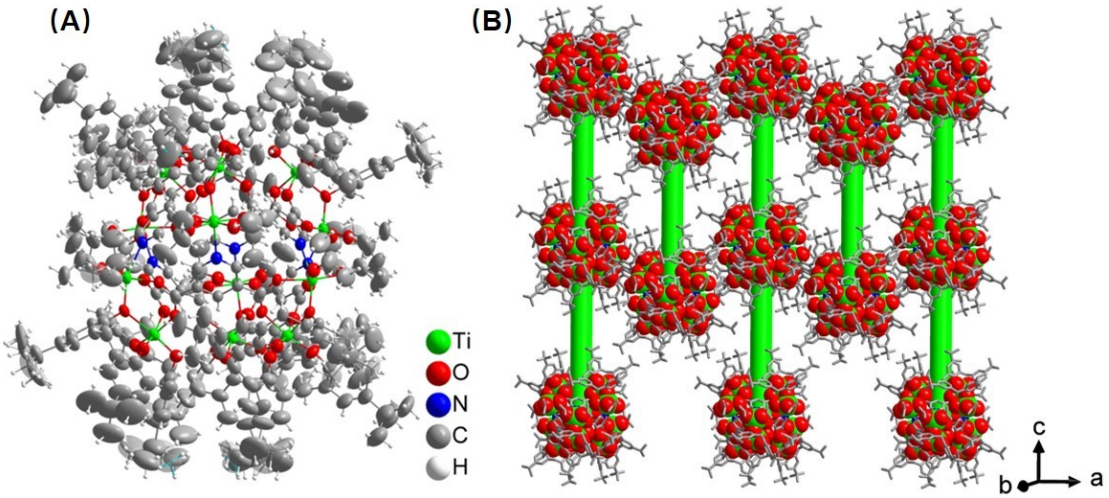

Figure S8. (A) ORTEP representation of the structure of **{$Ti_{12}L_6$-1}**; (B) Three-dimensional packing structure of **{$Ti_{12}L_6$-1}**. The cages are stacked to form uniform nanotubes in a face-to-face fashion along the *c* direction.

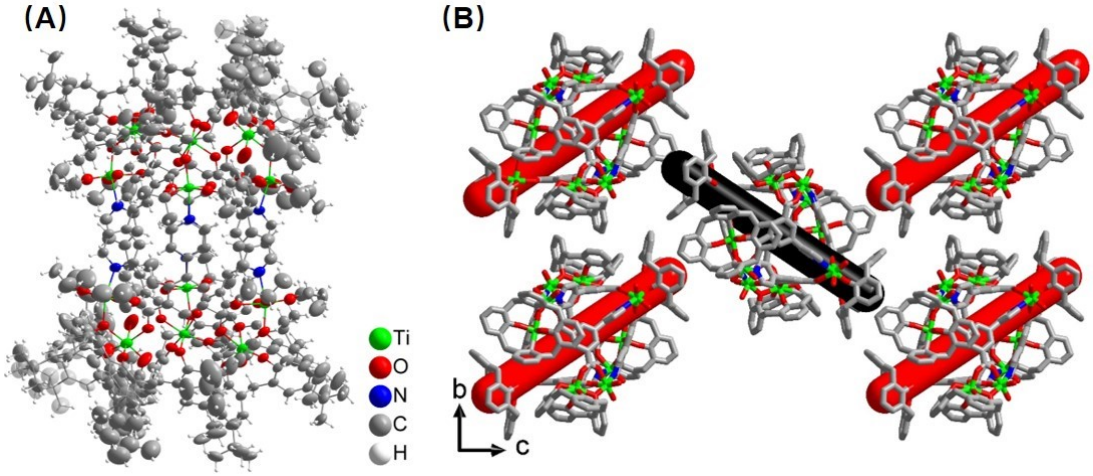

Figure S9. (A) ORTEP representation of the structure of **{$Ti_{12}L_6$-2}**; (B) Three-dimensional packing structure of **{$Ti_{12}L_6$-2}**.

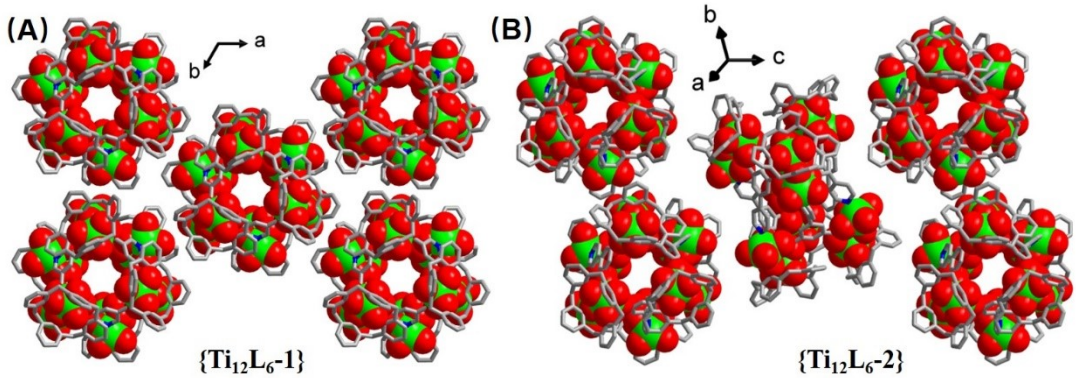

Figure S10. Comparison of stacking patterns of **{$Ti_{12}L_6$-1}**(A) and **{$Ti_{12}L_6$-2}**(B)**.**

3. Powder X-ray Diffraction

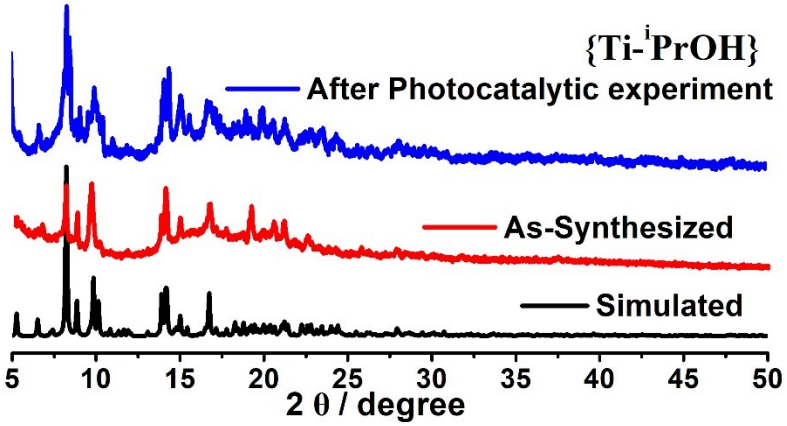

Figure S11. The XRD patterns of **{Ti-^{i}PrOH}**.

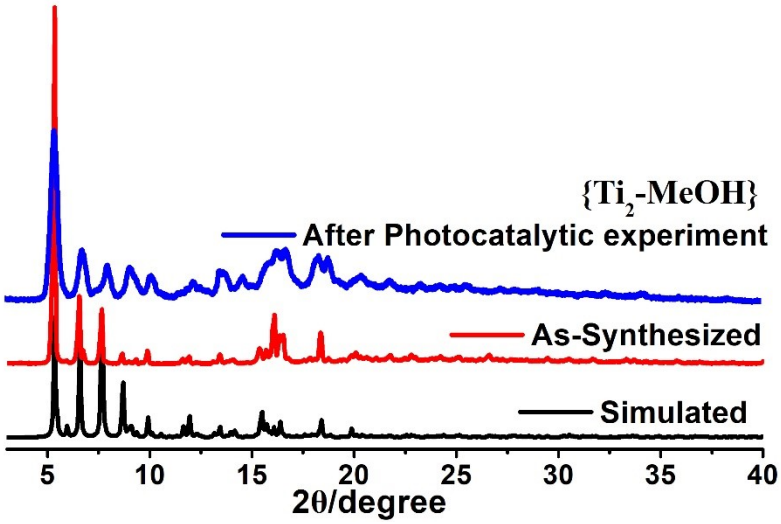

Figure S12. The XRD patterns of **{Ti_2-MeOH}**.

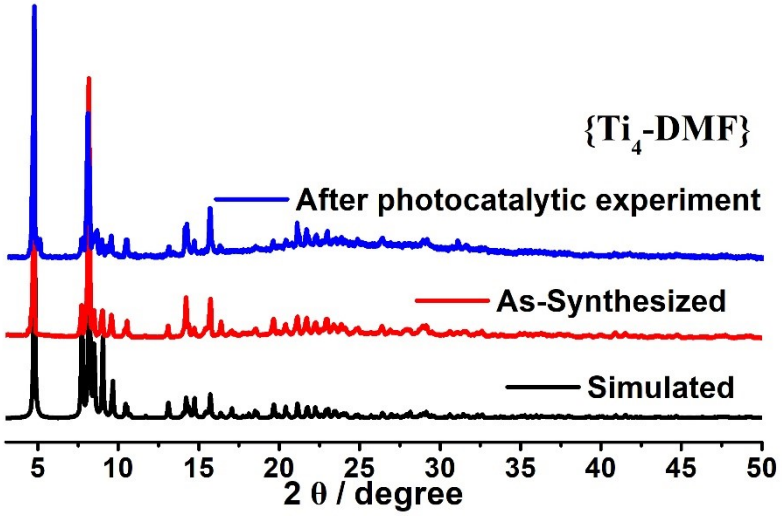

Figure S13. The XRD patterns of **{Ti_4-DMF}**.

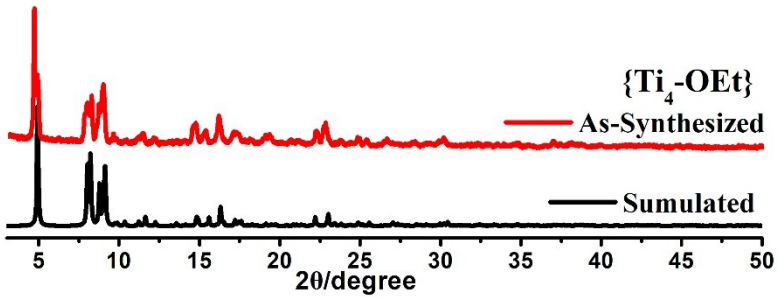

Figure S14. The XRD patterns of **{Ti$_4$-EtOH}**.

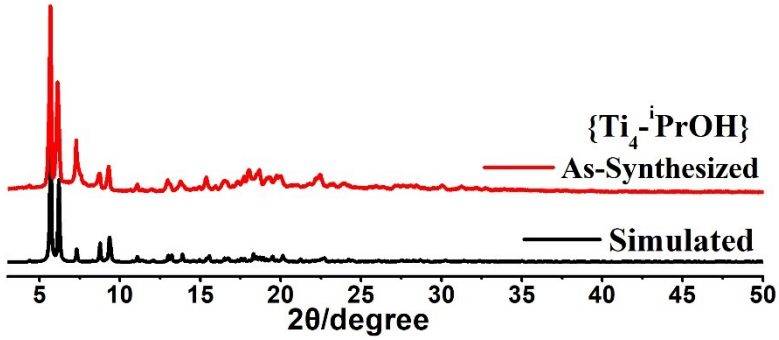

Figure S15. The XRD patterns of **{Ti$_4$-^{i}PrOH}**.

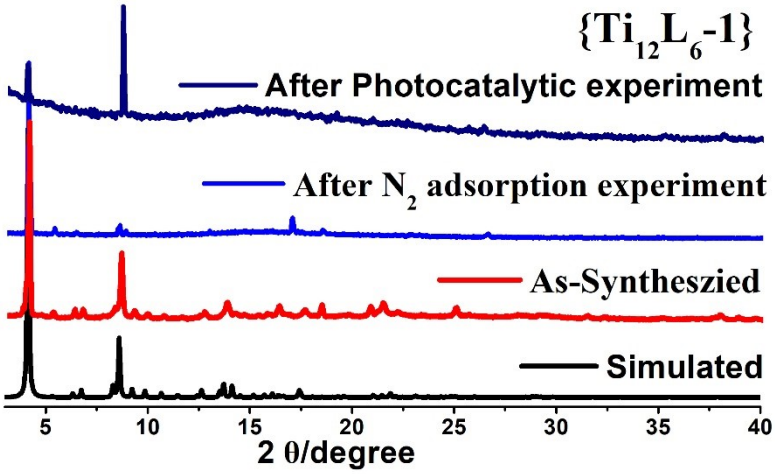

Figure S16. The XRD patterns of **{Ti$_{12}$L$_6$-1}**.

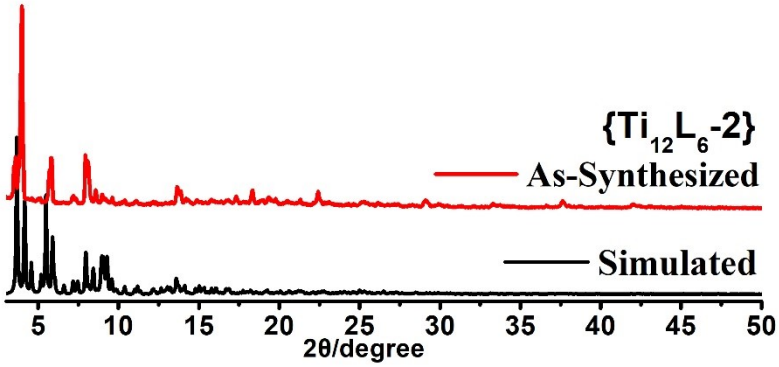

Figure S17. The XRD patterns of **{Ti$_{12}$L$_6$-2}**.

4. XPS Tests

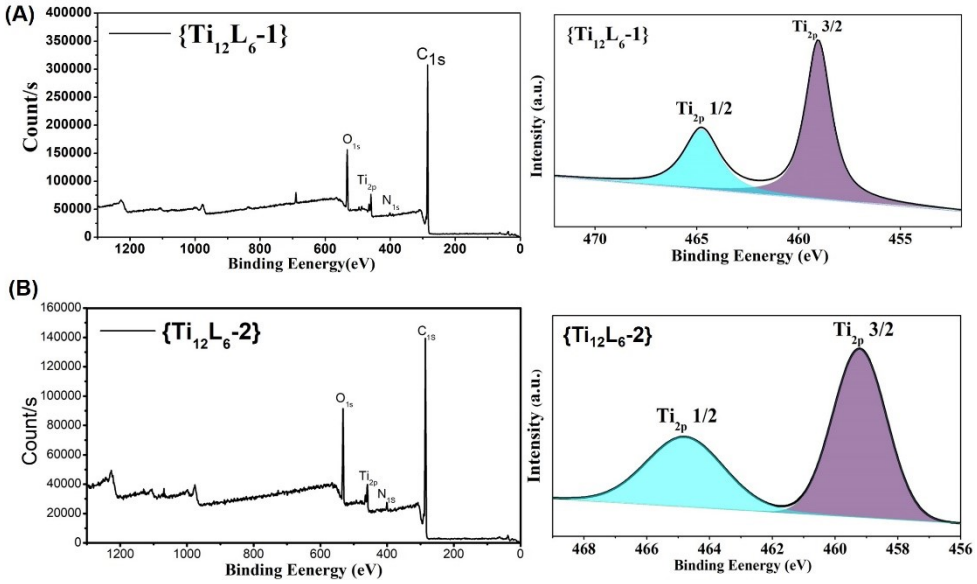

Figure S18. XPS tests of **{$Ti_{12}L_6$-1}** and **{$Ti_{12}L_6$-2}**.

4. N_2 Sorption Isotherm.

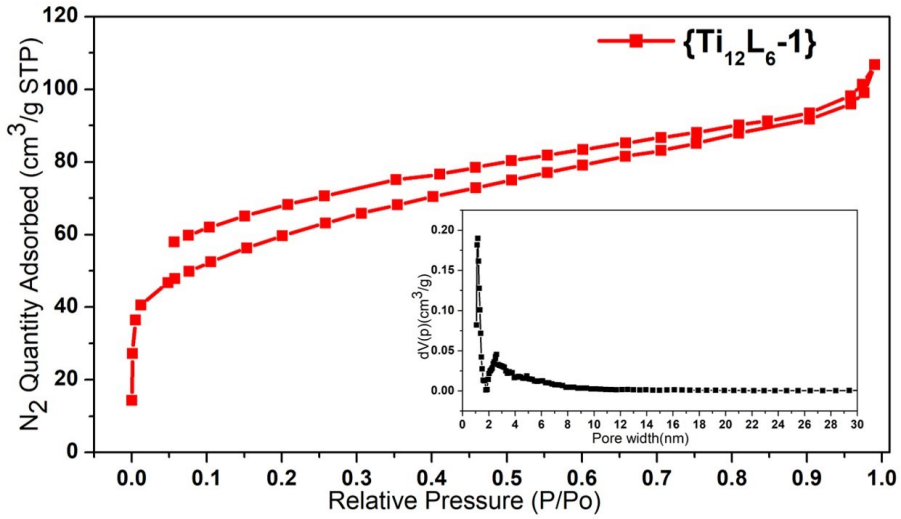

Figure S19. N_2 sorption isotherms of **{$Ti_{12}L_6$-1}**. **{$Ti_{12}L_6$-2}** has a low yield (less than 5%) and coexists with other impurities. We can only manually pick a small number of crystals to do some basic characterization. However, at least 80 mg of samples are needed for BET experiments, and we cannot get so many samples.

6. Energy Dispersive X-ray (EDX) Spectroscopic Analysis

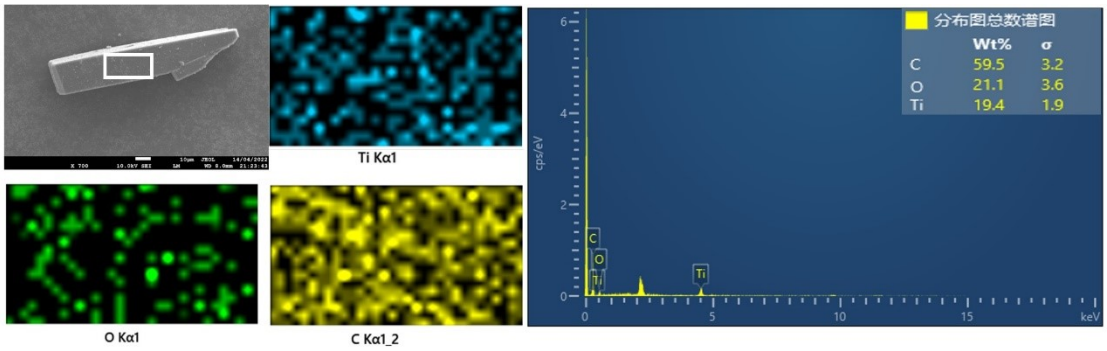

Figure S20. The EDS pattern of **{Ti-^{i}PrOH}**.

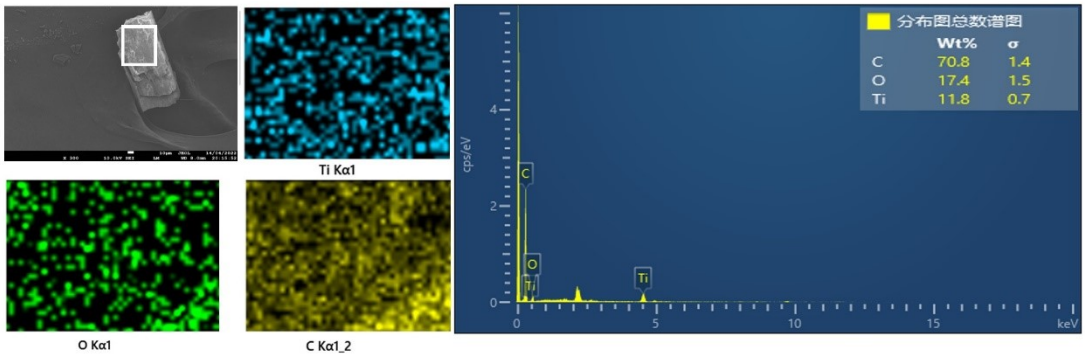

Figure S21. The EDS pattern of **{Ti_2-MeOH}**.

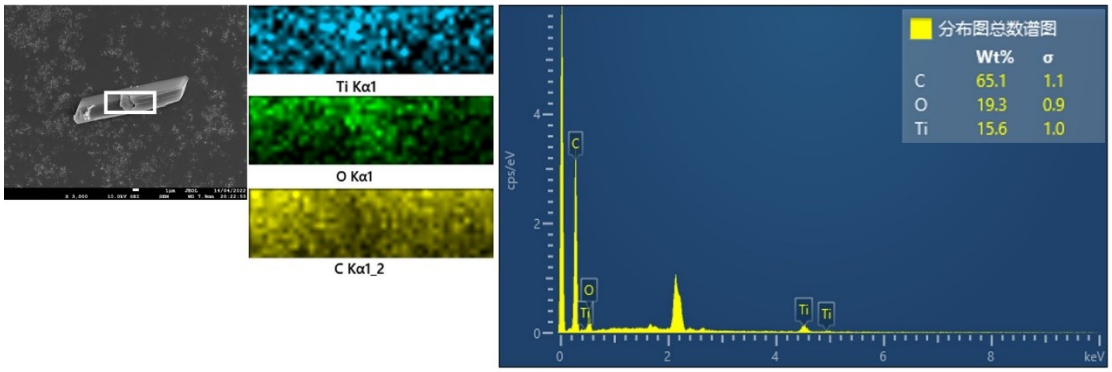

Figure S22. The EDS pattern of **{Ti_4-DMF}**.

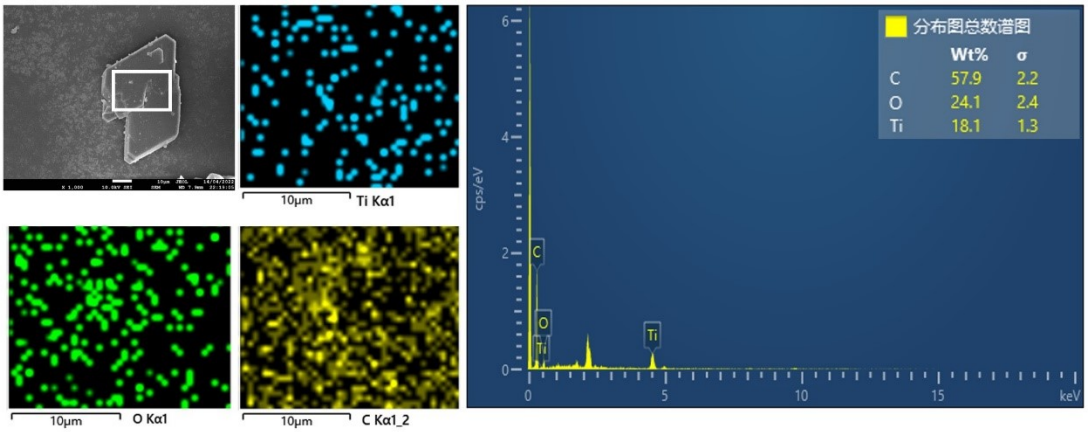

Figure S23. The EDS pattern of **{Ti_4-EtOH}.**

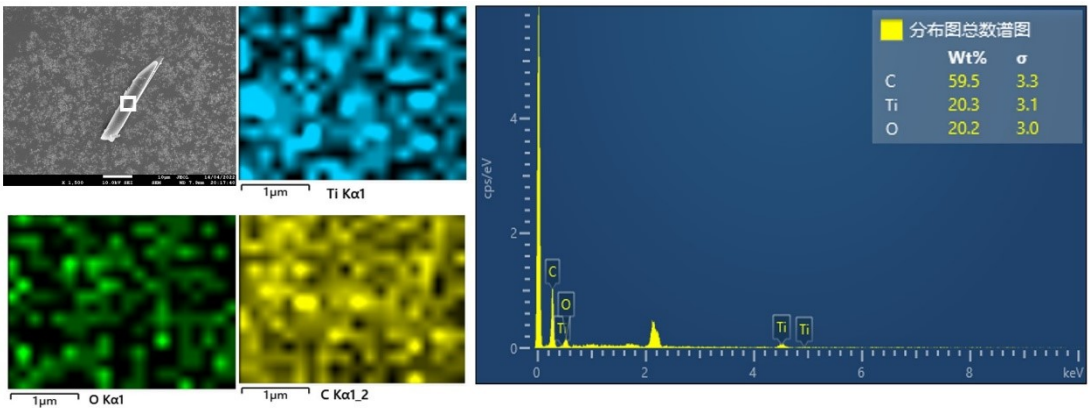

Figure S24. The EDS pattern of **{Ti_4-^{i}PrOH}.**

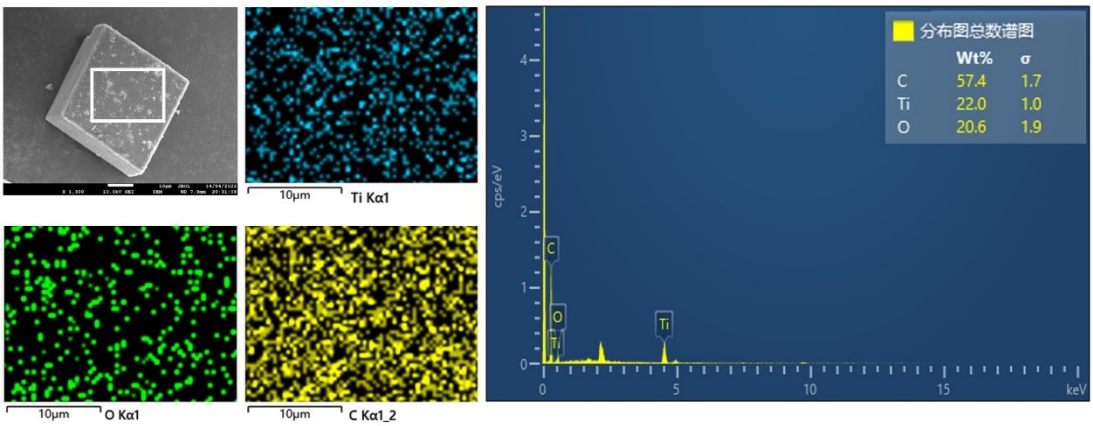

Figure S25. The EDS pattern of **{$Ti_{12}L_6$-1}**.

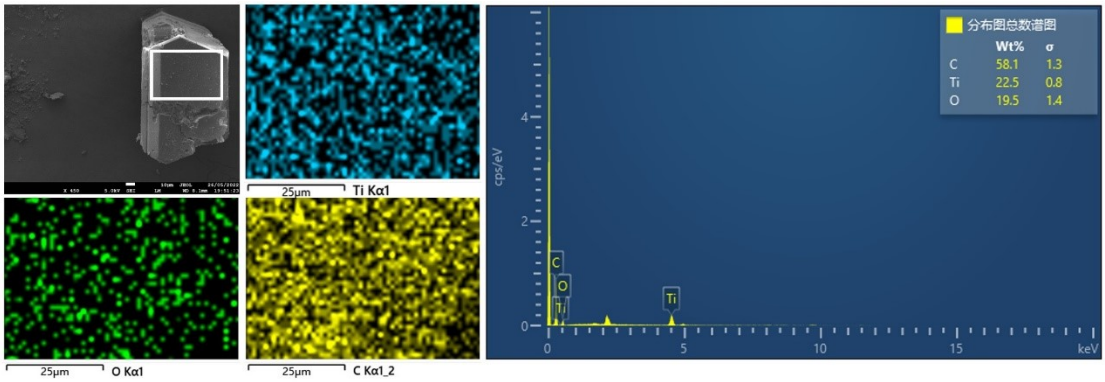

Figure S26. The EDS pattern of **{$Ti_{12}L_6$-2}**.

8. TG-Measurement

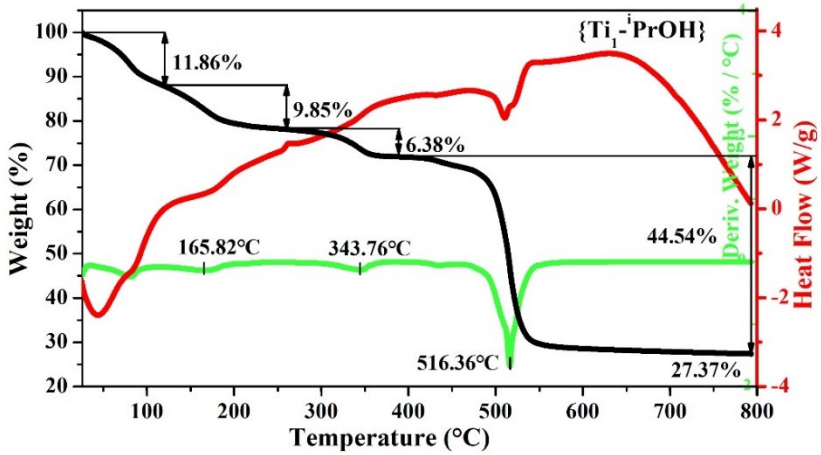

Figure S27. The TGA and DSC curves of **{Ti-^{i}PrOH}**.

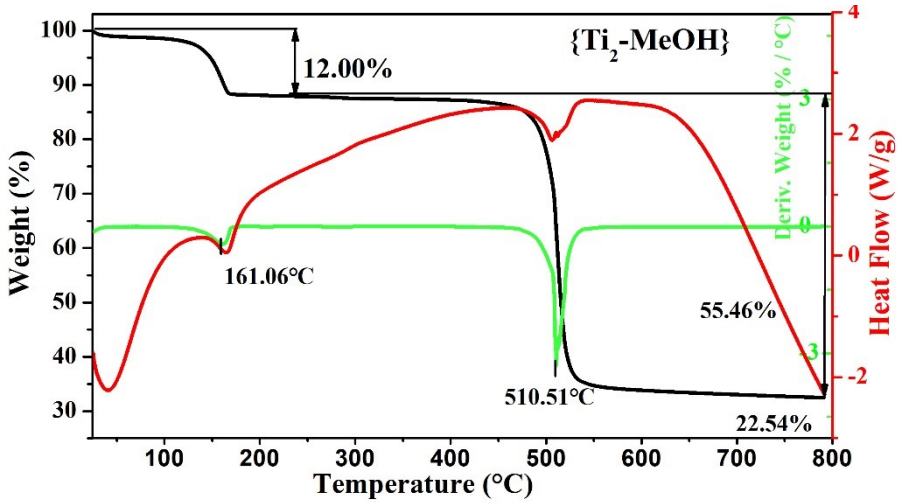

Figure S28. The TGA and DSC curves of **{Ti_2-MeOH}**.

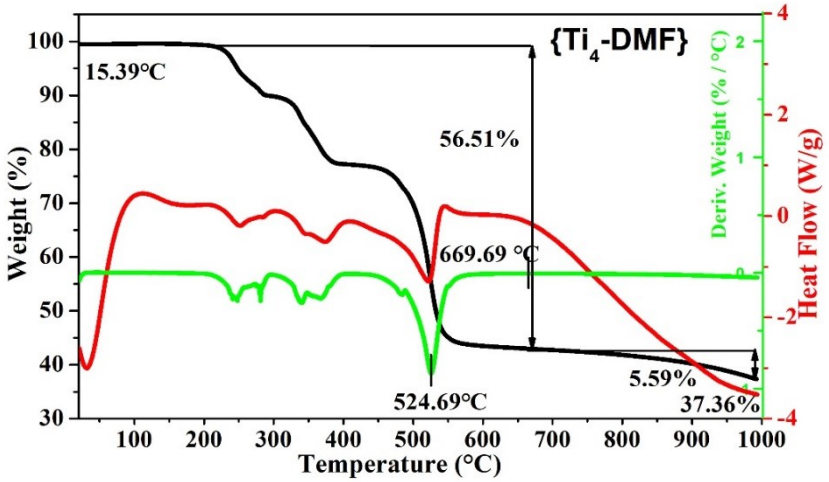

Figure S29. The TGA and DSC curves of **{Ti_4-DMF}**.

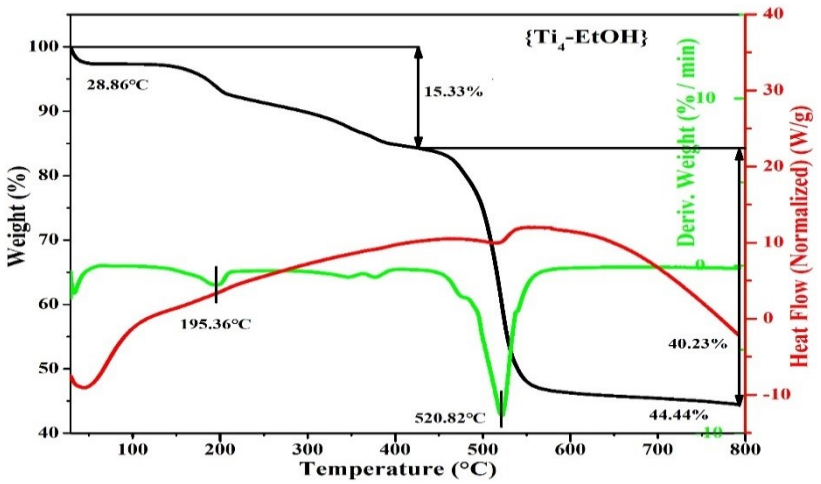

Figure S30. The TGA and DSC curves of **{Ti_4-EtOH}**.

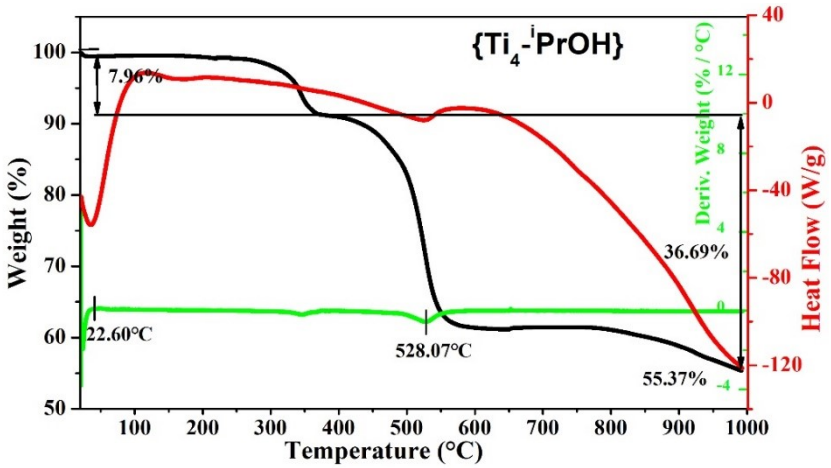

Figure S31. The TGA and DSC curves of **{Ti_4-^{i}PrOH}**.

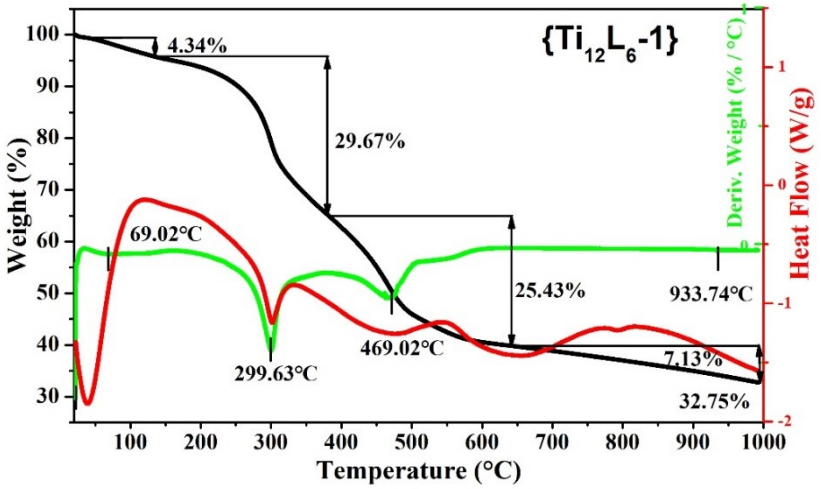

Figure S32. The TGA and DSC curves of **{$Ti_{12}L_6$-1}**.

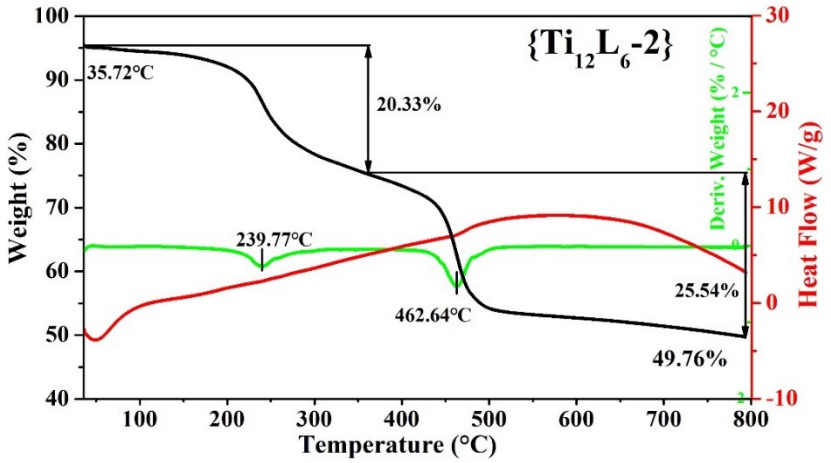

Figure S33. The TGA and DSC curves of **{$Ti_{12}L_6$-2}**.

7. IR Spectra

Figure S34-40 shows the FTIR spectra of clusters. The broad band between 3200-3500 cm^{-1} attributable to OH stretching. The strong vibration band at ca. 1620-1650 cm^{-1} can be ascribed to C=O stretching of the carboxyl. The characteristic bands of Ti-O-C and Ti-O-Ti appears in the ranges of 1000–1200 and 700–800 cm^{-1}, respectively.

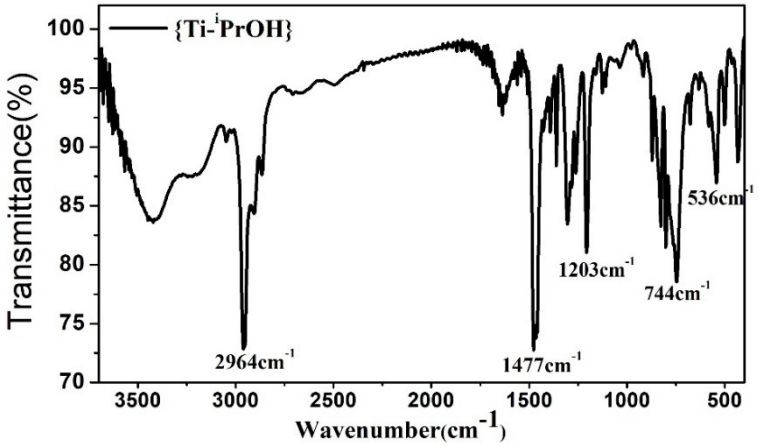

Figure S34. IR spectrum of crystal sample of **{Ti-^{i}PrOH}**.

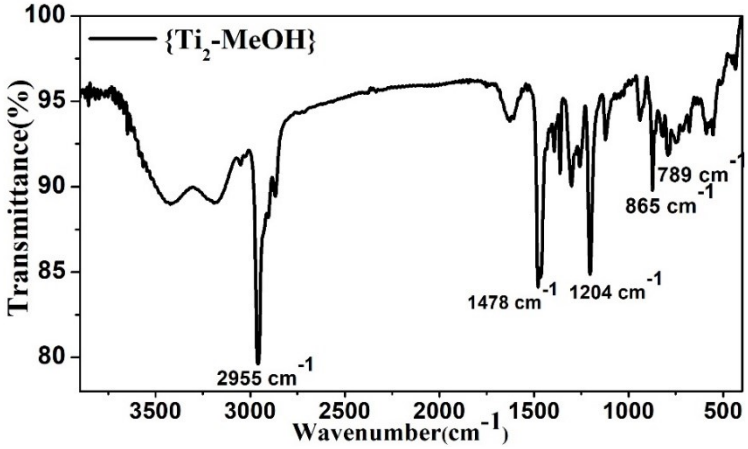

Figure S35. IR spectrum of crystal sample of **{Ti_2-MeOH}**.

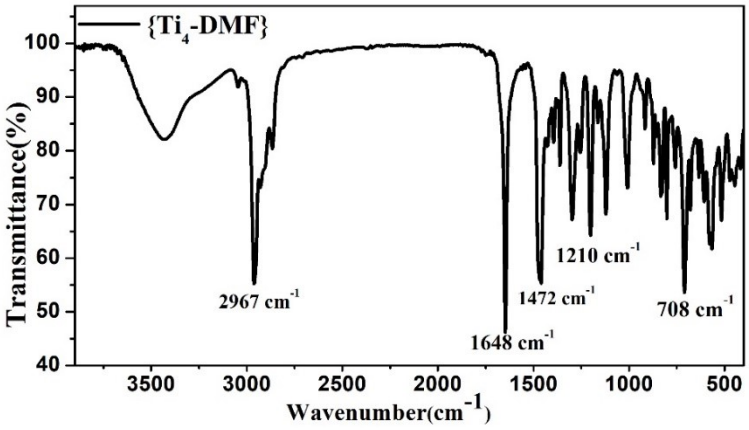

Figure S36. IR spectrum of crystal sample of **{Ti_4-DMF}**.

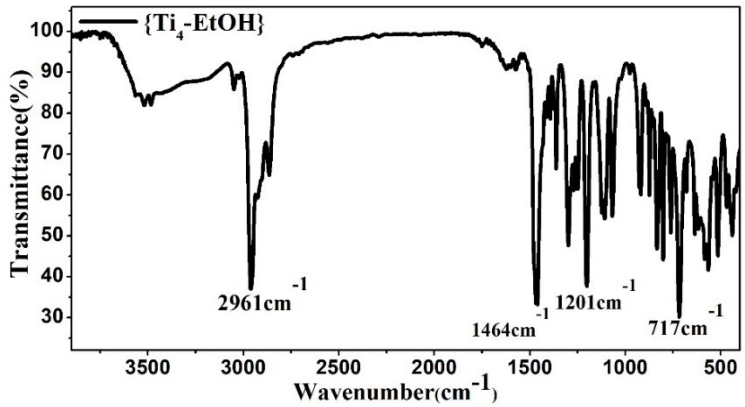

Figure S37. IR spectrum of crystal sample of **{Ti_4-EtOH}**.

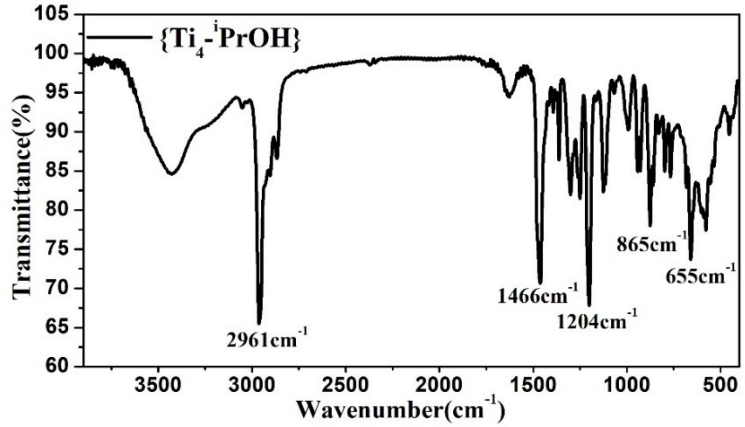

Figure S38. IR spectrum of crystal sample of **{Ti_4-^{i}PrOH}**.

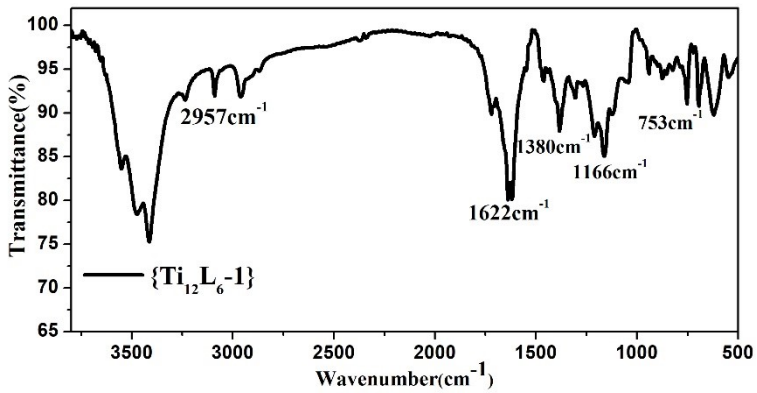

Figure S39. IR spectrum of crystal sample of **{$Ti_{12}L_6$-1}**.

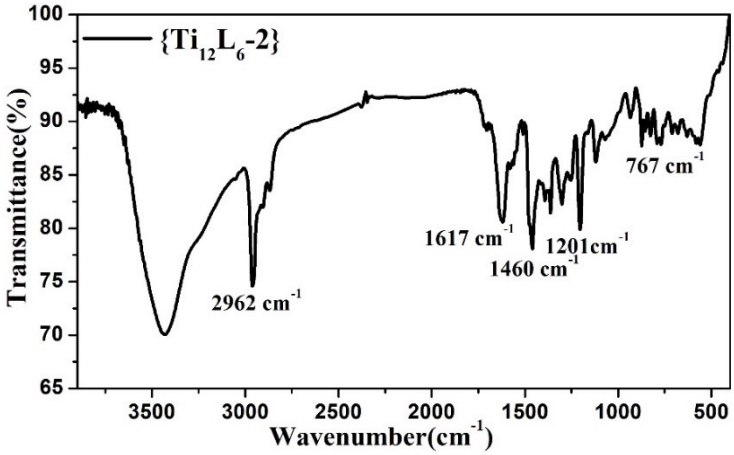

Figure S40. IR spectrum of crystal sample of **{$Ti_{12}L_6$-2}**.

8. Contact Angle Tests

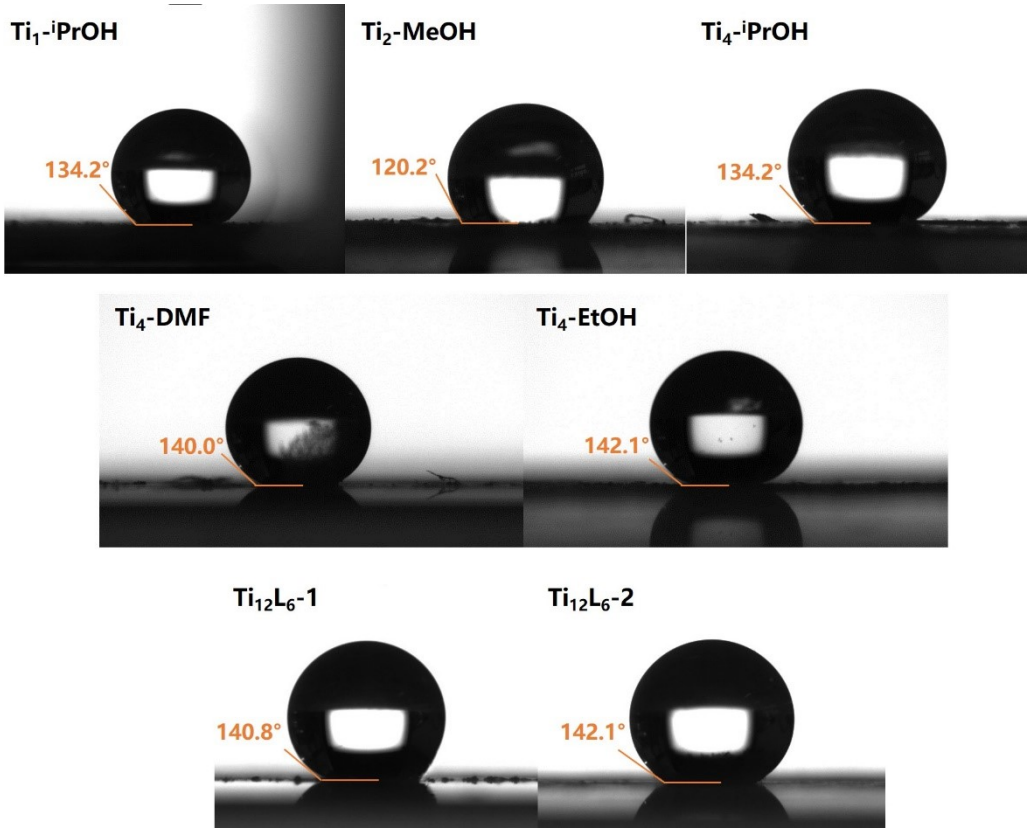

Figure S41. Contact angle pattern for the clusters and cages.

9. ESI-MS *Measurements.*

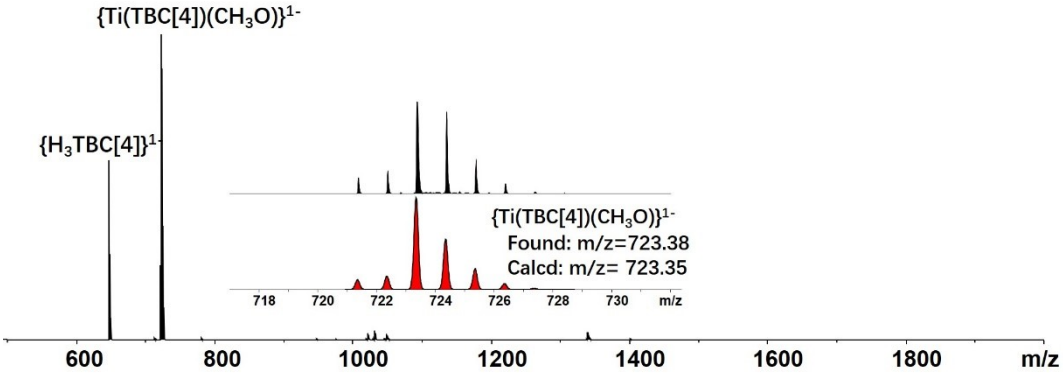

Figure S42. ESI-MS spectrum of the CH_3OH solution of **{Ti-^{i}PrOH}**.

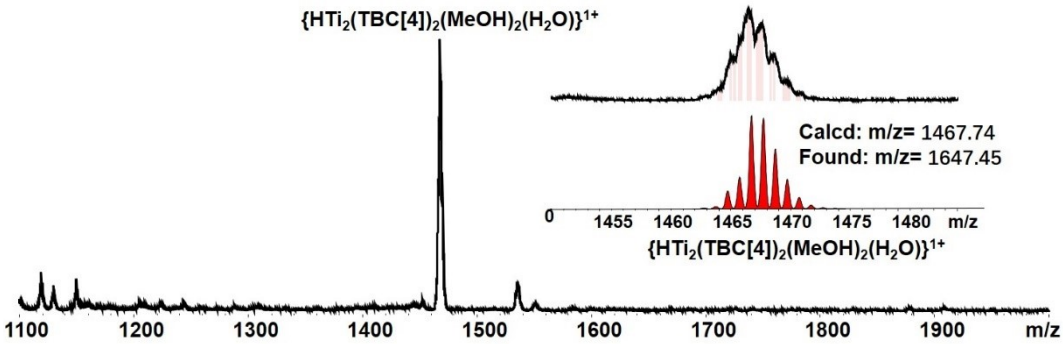

Figure S43. ESI-MS spectrum of the CH_3OH solution of **{Ti_2-MeOH}**.

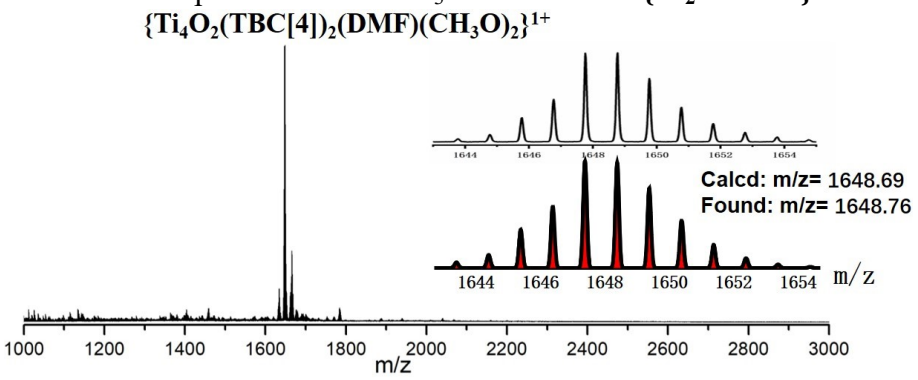

Figure S44. ESI-MS spectrum of the CH_3OH solution of **{Ti_4-DMF}**.

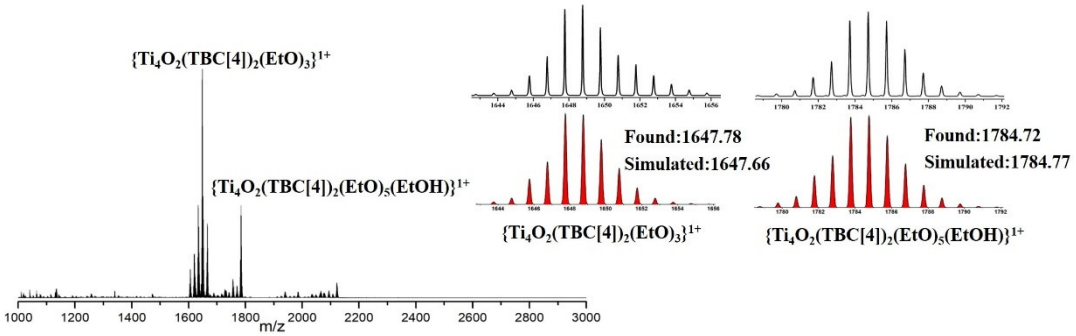

Figure S45. ESI-MS spectrum of the CH_3OH solution of **{Ti_4-EtOH}**.

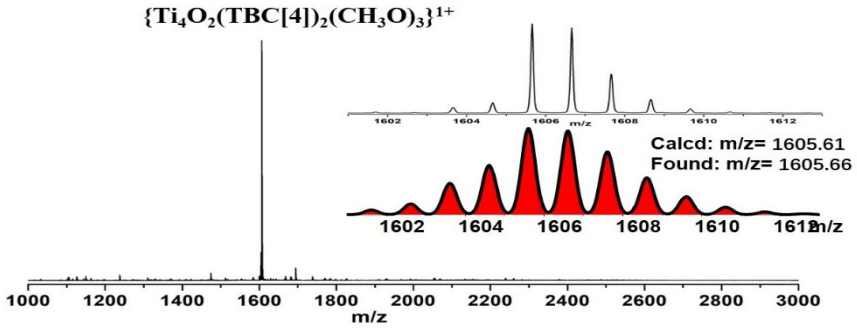

Figure S46. ESI-MS spectrum of the CH_3OH solution of **{Ti_4-^{i}PrOH}**.

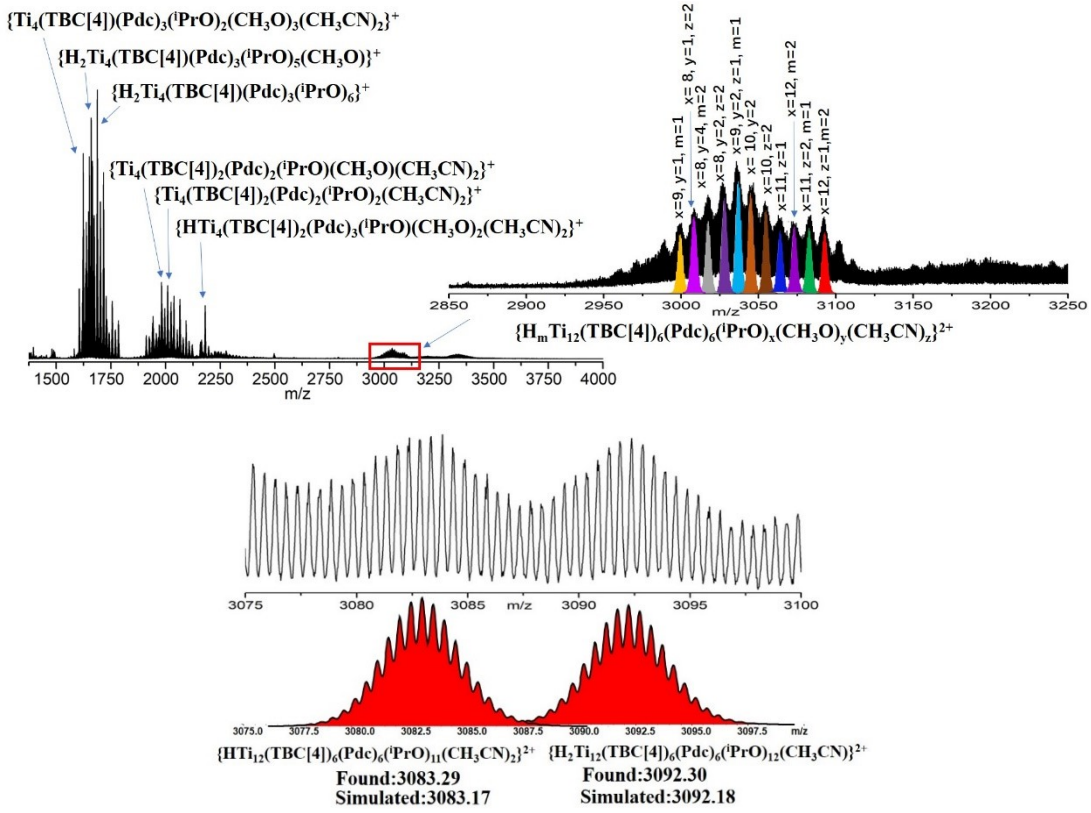

Figure S47. ESI-MS spectra of the CH_3OH solution of **{$Ti_{12}L_6$-1}**.

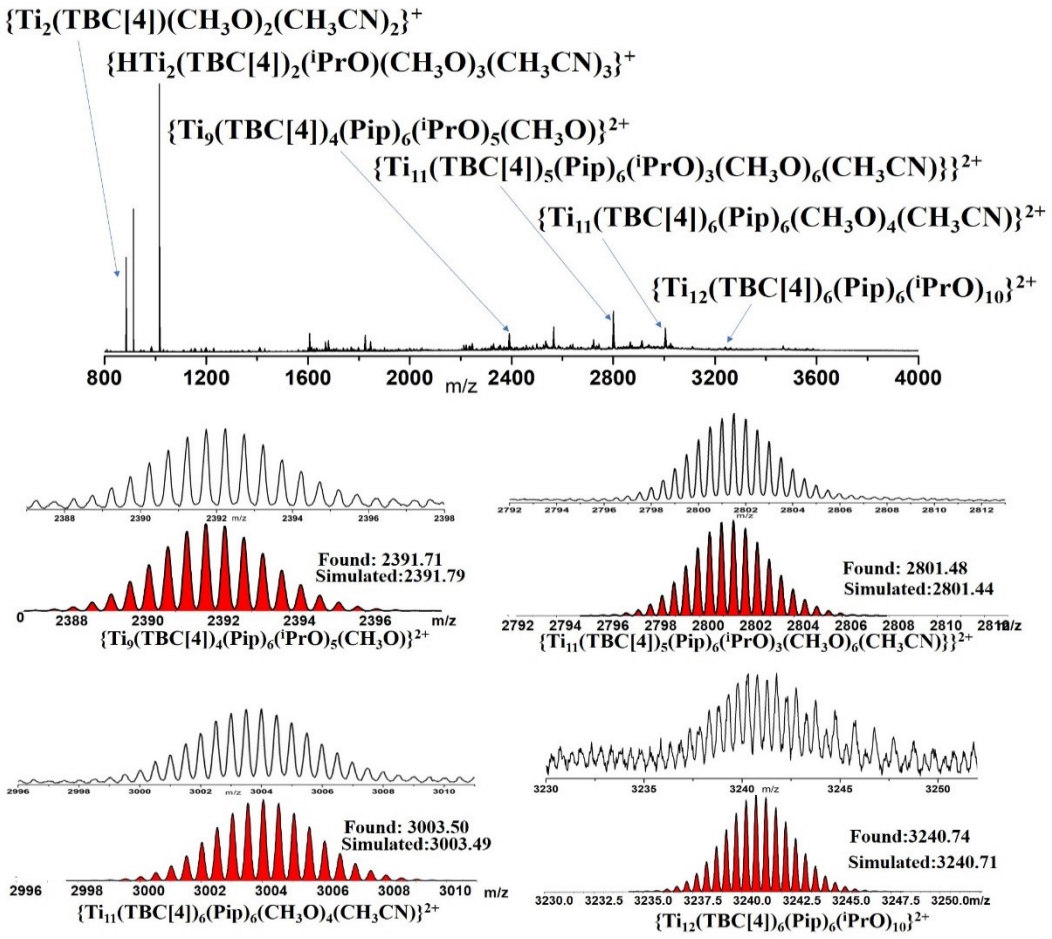

Figure S48. ESI-MS spectra of the CH_3OH solution of **{$Ti_{12}L_6$-2}**.

9. Band-gap investigation

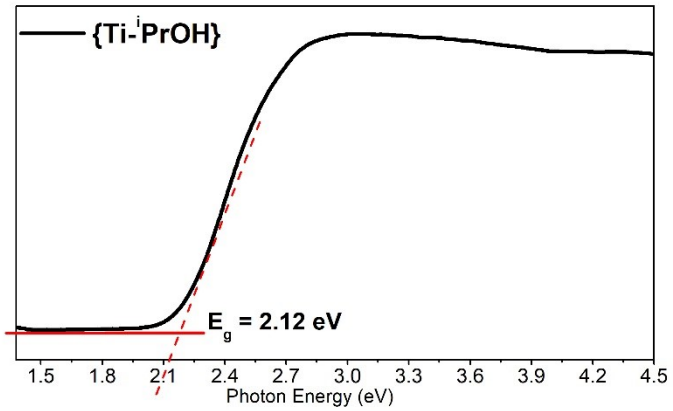

Figure 49. Kubelka–Munk transformation of diffuse reflectance data of **{Ti-^{i}PrOH}**.

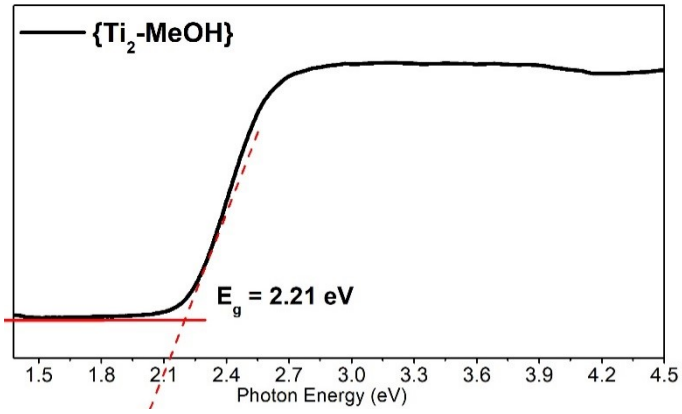

Figure 50. Kubelka–Munk transformation of diffuse reflectance data of **{Ti_2-MeOH}**.

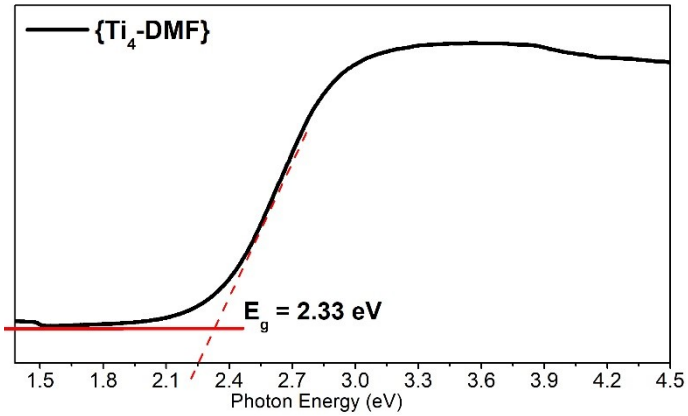

Figure 51. Kubelka–Munk transformation of diffuse reflectance data of **{Ti_4-DMF}**.

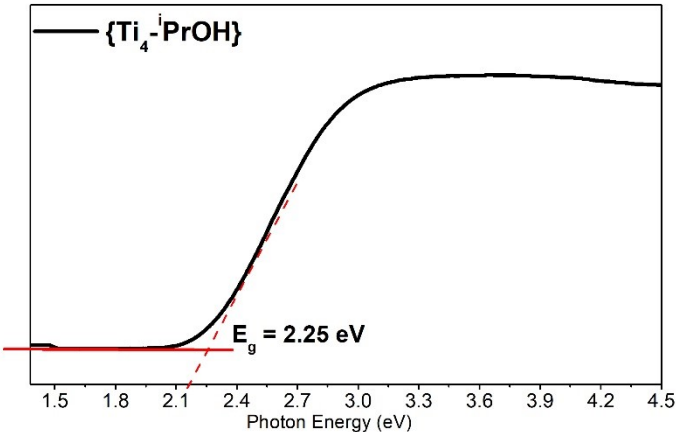

Figure 52. Kubelka–Munk transformation of diffuse reflectance data of **{Ti_4-^{i}PrOH}**.

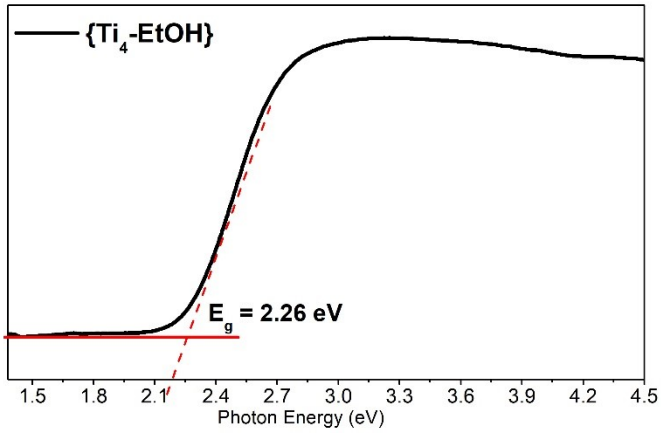

Figure 53. Kubelka–Munk transformation of diffuse reflectance data of **{Ti_4-EtOH}**.

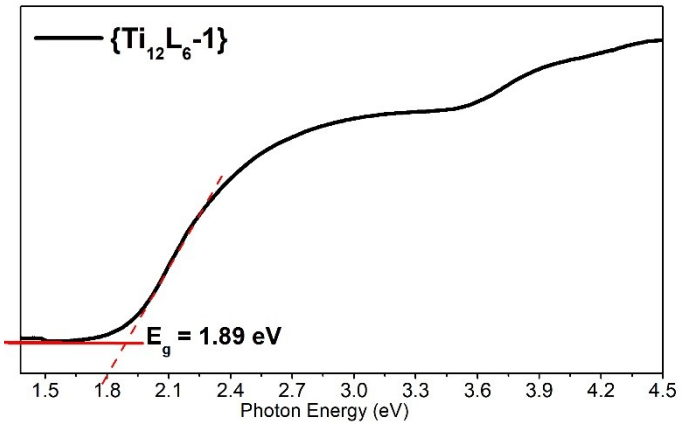

Figure 54. Kubelka–Munk transformation of diffuse reflectance data of **{$Ti_{12}L_6$-1}**.

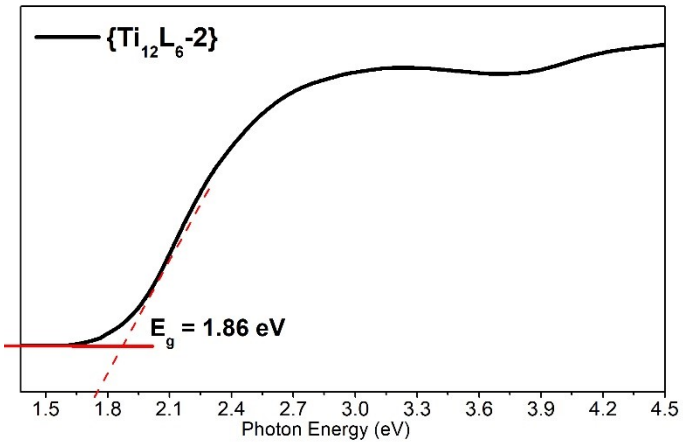

Figure 55. Kubelka–Munk transformation of diffuse reflectance data of **{$Ti_{12}L_6$-2}**.

10. H_2 Evolution Study.

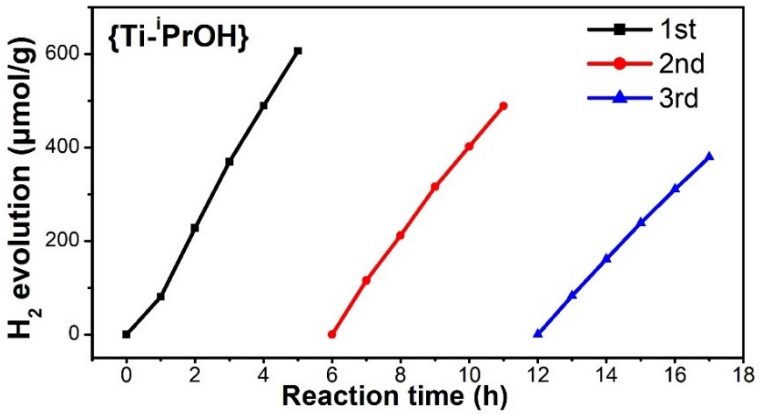

Figure S56. Recycling H_2 evolution experiments of **{Ti-^{i}PrOH}.**

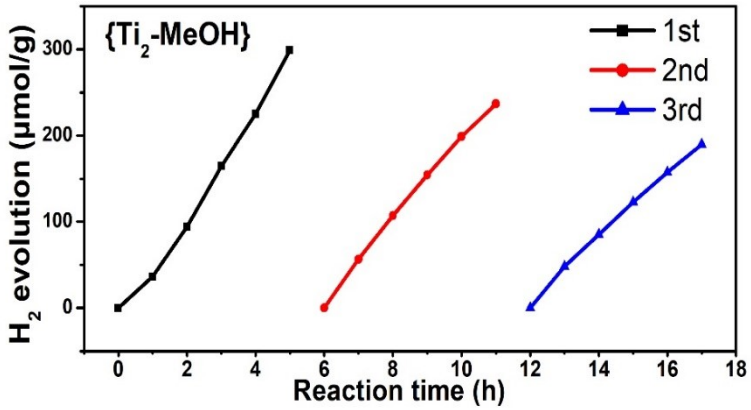

Figure S57. Recycling H_2 evolution experiments of **{Ti_2-MeOH}.**

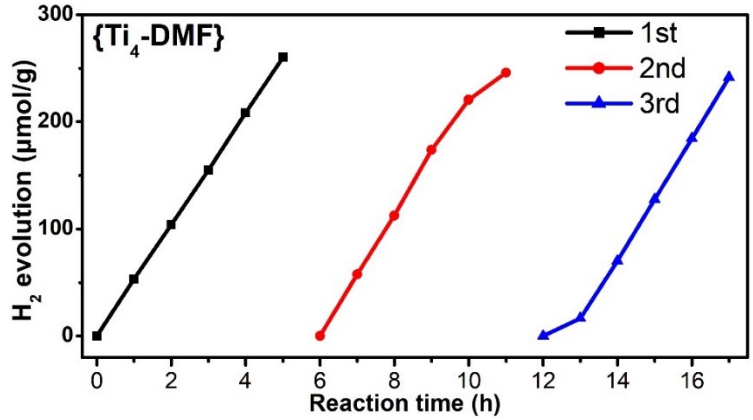

Figure S58. Recycling H_2 evolution experiments of **{Ti_4-DMF}**

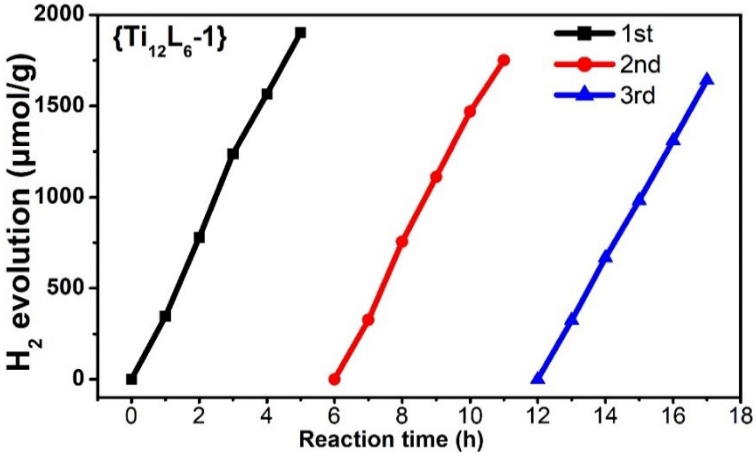

Figure S59. Recycling H_2 evolution experiments of **{$Ti_{12}L_6$-1}**.

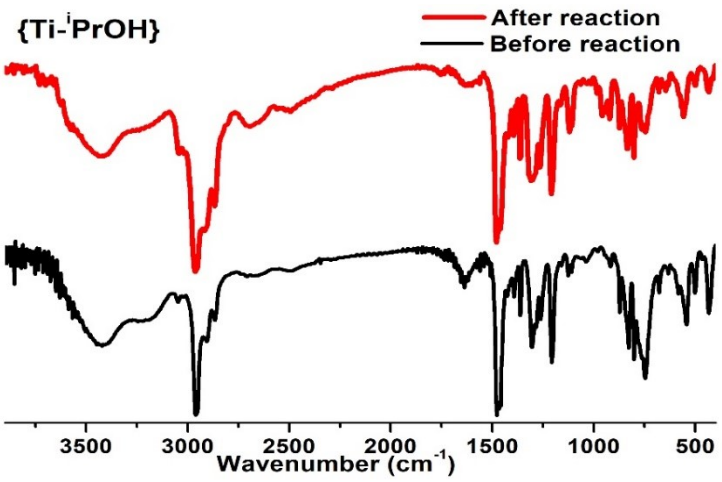

Figure S60. IR spectrum of {**Ti-^{i}PrOH**} before and after photocatalytic reaction.

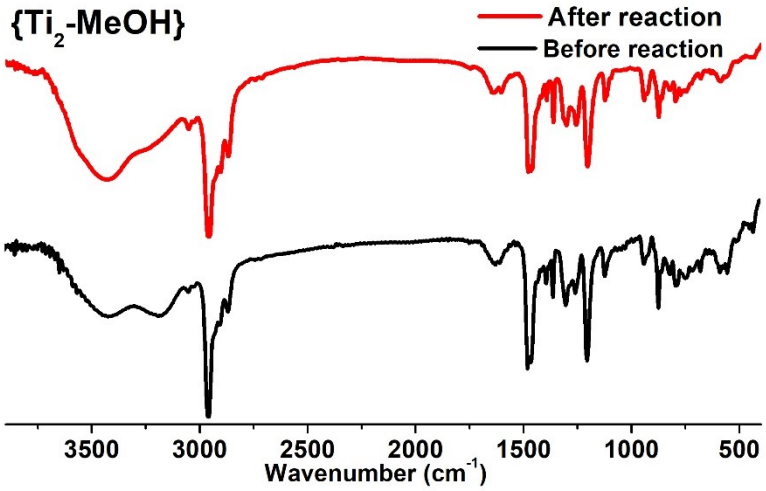

Figure S61. IR spectrum of {**Ti$_2$-MeOH**} before and after photocatalytic reaction.

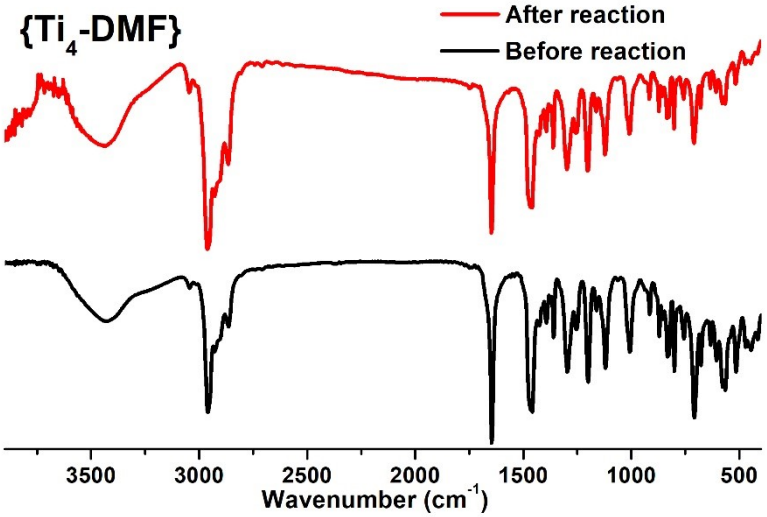

Figure S62. IR spectrum of {**Ti$_4$-DMF**} before and after photocatalytic reaction.

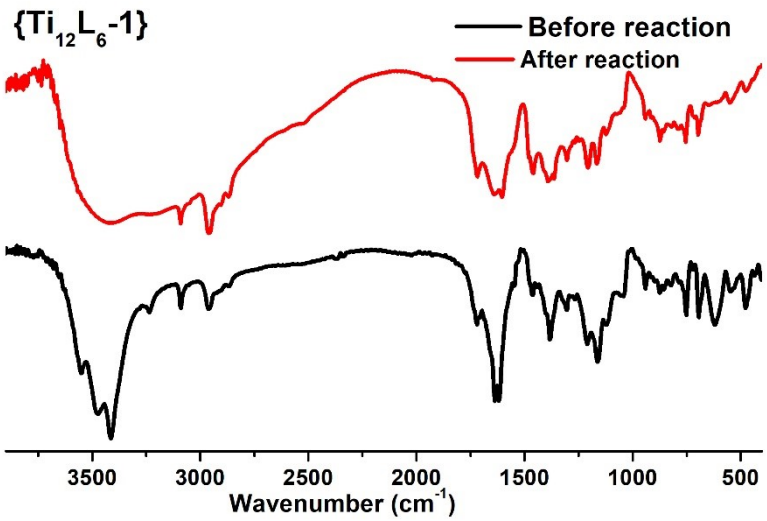

Figure S63. IR spectrum of **{$Ti_{12}L_6$-1}** before and after photocatalytic reaction.

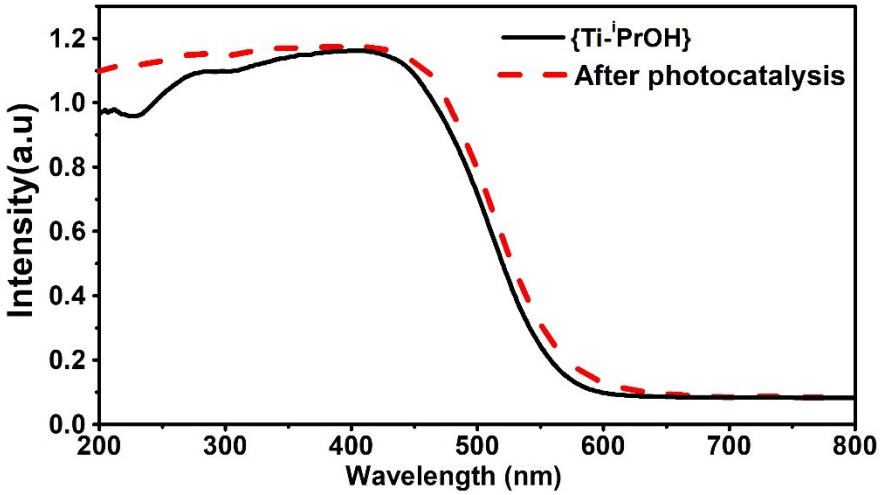

Figure S64. Solid-state UV-vis spectra of **{Ti-^{i}PrOH}** and sample after photocatalytic experiment.

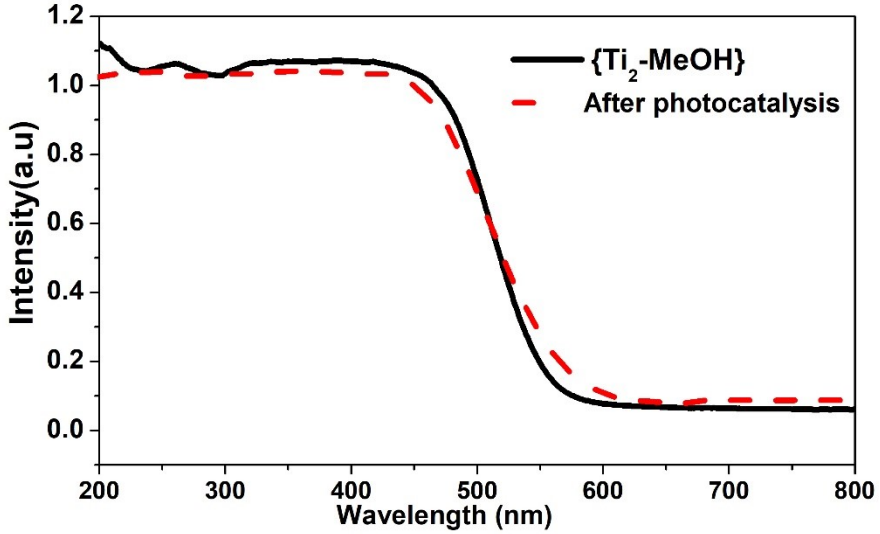

Figure S65. Solid-state UV-vis spectra of **{Ti_2-MeOH}** and sample after photocatalytic experiment.

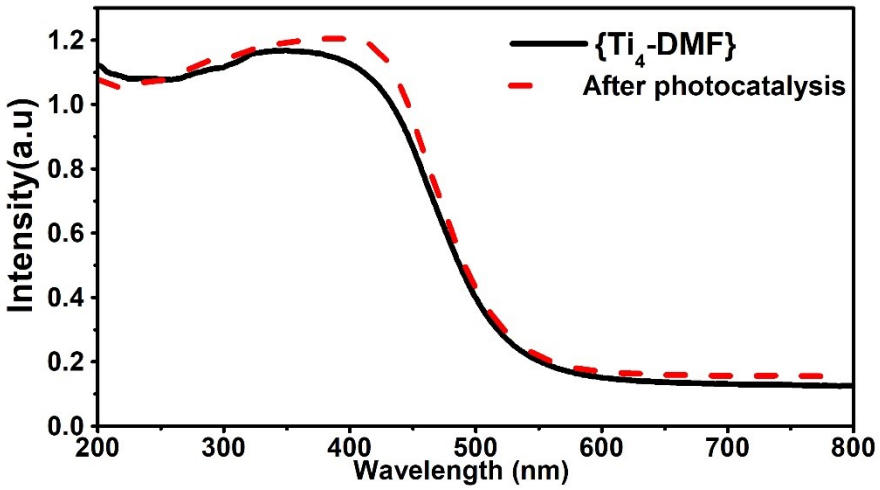

Figure S66. Solid-state UV-vis spectra of {**Ti_4-DMF**} and sample after photocatalytic experiment.

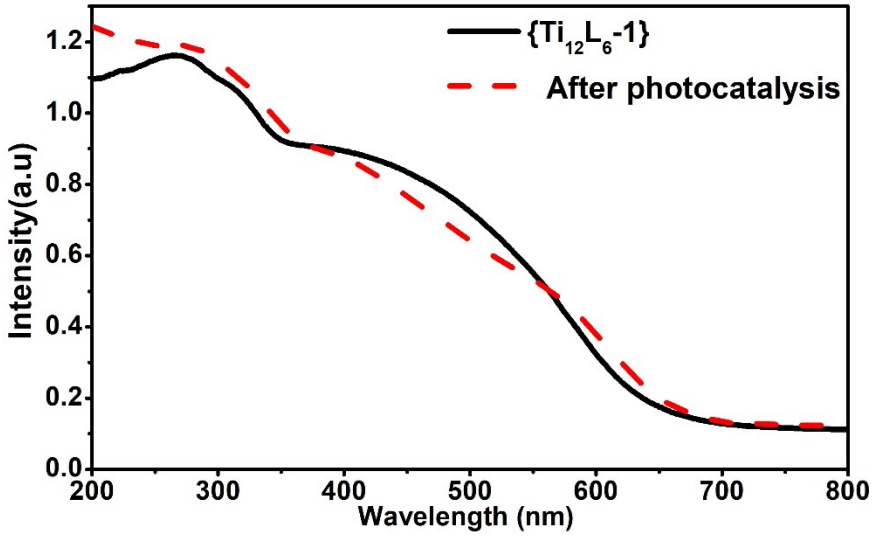

Figure S67. Solid-state UV-vis spectra of {**$Ti_{12}L_6$-1**} and sample after photocatalytic experiment.

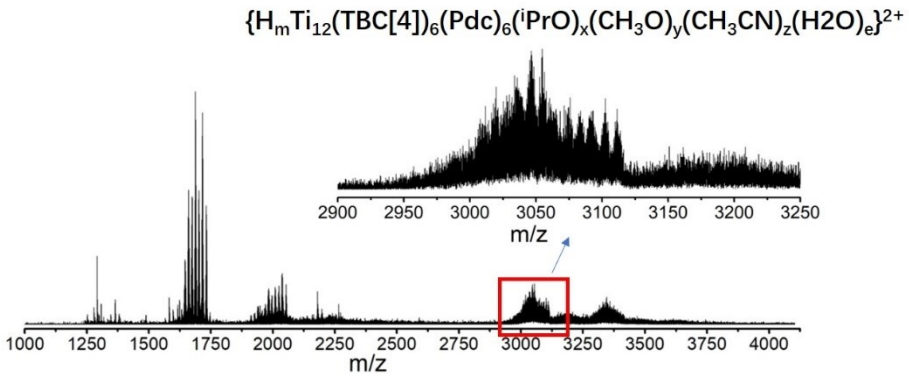

Figure S68. ESI-MS of {**$Ti_{12}L_6$-1**} after photocatalysis reaction.

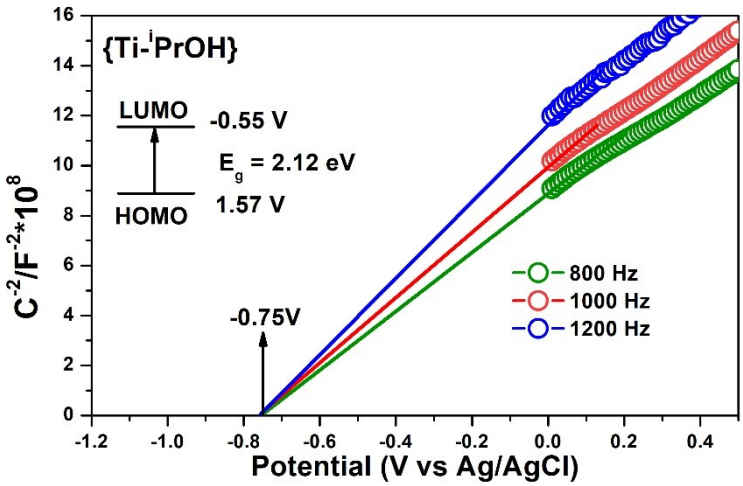

Figure 69. Mott–Schottky plot (insets are the estimated HOMO and LUMO levels of the cluster) of **{Ti-^{i}PrOH}**.

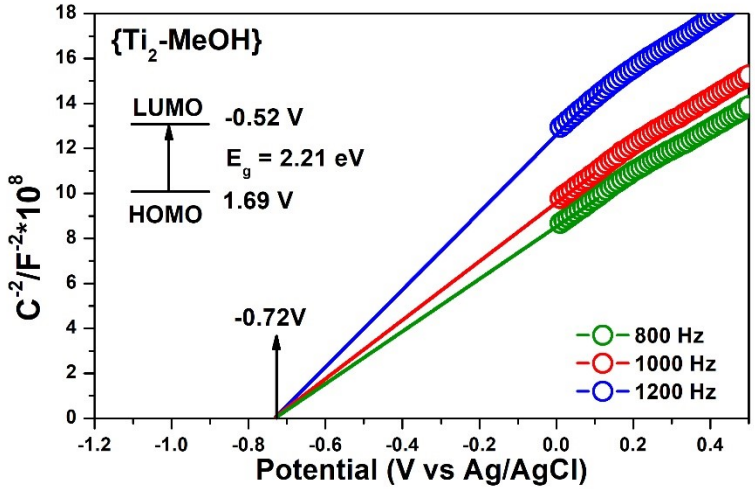

Figure 70. Mott–Schottky plot (insets are the estimated HOMO and LUMO levels of the cluster) of **{Ti_2-MeOH}**.

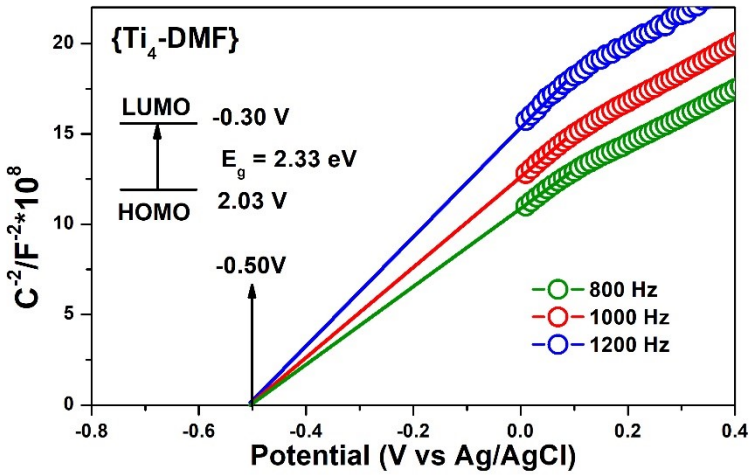

Figure 71. Mott–Schottky plot (insets are the estimated HOMO and LUMO levels of the cluster) of **{Ti_4-DMF}**.

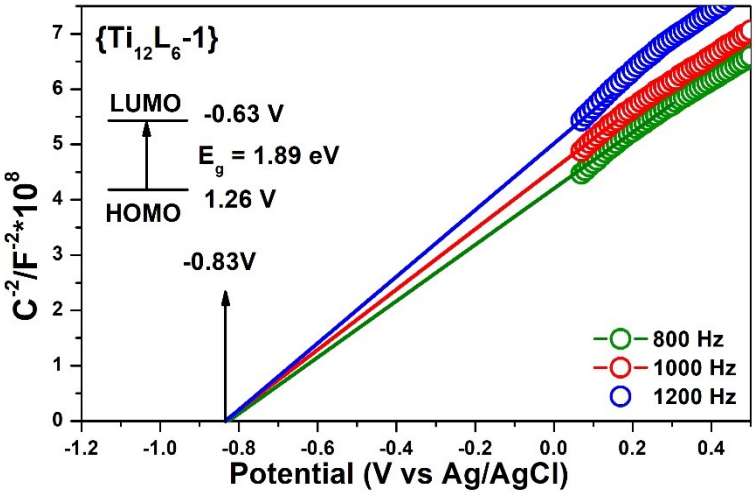

Figure 72. Mott−Schottky plot (insets are the estimated HOMO and LUMO levels of the cluster) of **{$Ti_{12}L_6$-2}**.

10. DFT Calculation.

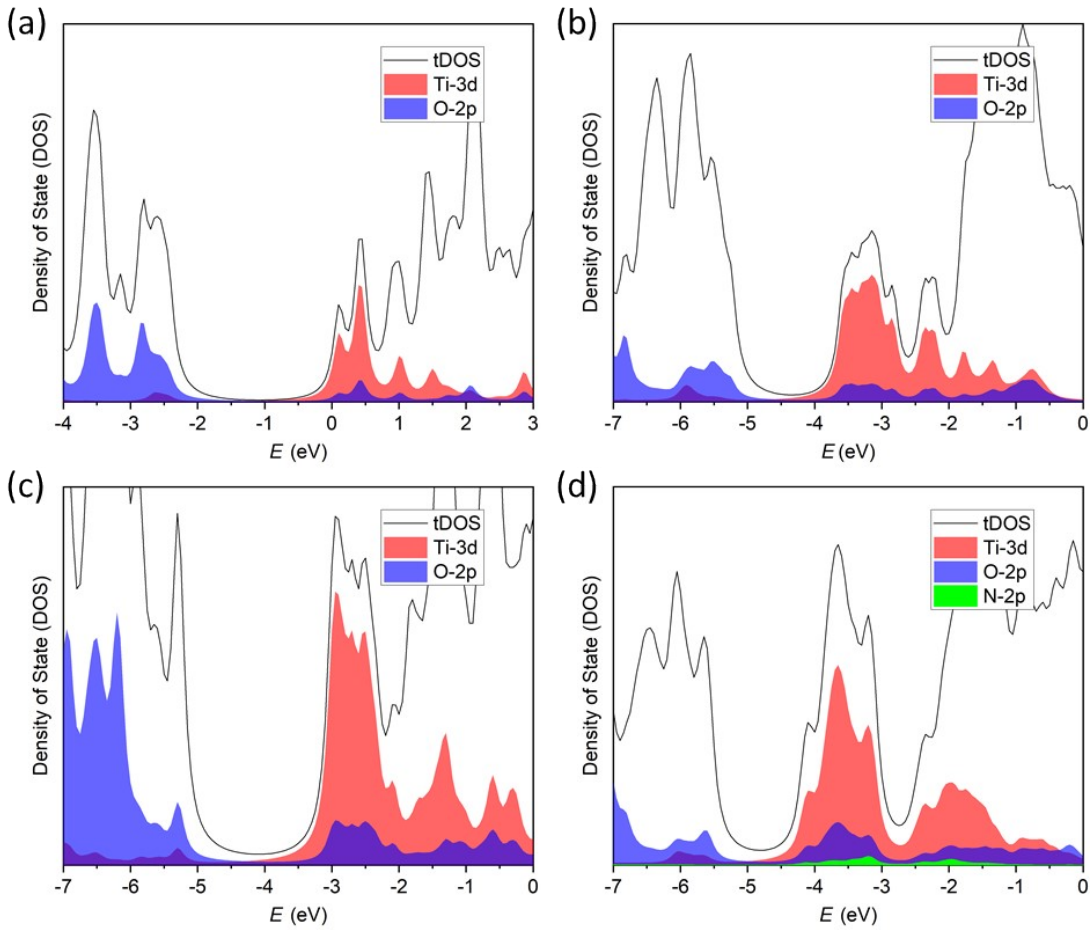

Figure S73. Total density of states (tDOS) and partial DOS (pDOS) for several atomic orbitals (AOs) in (a) **{Ti-^{i}PrOH}**, (b) **{Ti_2-MeOH}**, (c) **{Ti_4-DMF}** and (d) **{$Ti_{12}L_6$-1}**.

Table S2. Orbital energies of HOMO, LUMO and ΔE_{HL} of the two cluster cages.

Energy / eV	E_{HOMO}	E_{LUMO}	ΔE_{HL}
{Ti_4-DMF}	-5.265	-3.013	2.252
{$Ti_{12}L_6$-1}	-5.558	-4.175	1.383